ChemPhysChem

Research Article
doi.org/10.1002/cphc.202400921

Chemistry Europe
European Chemical Societies Publishing

www.chemphyschem.org

Valence Electron Count-Based Density Functional Theory to Investigate Structural Stability, Optoelectronic and Thermoelectric Properties of New p-Type Half-Heusler ZrYAu (Y = B, Al) Alloys

Radja Nour El Imene Bennoui,[a] Walid Adli,[a] Y. Al-Douri,*[b, c, d] Fadila Belkharroubi,[a] Fatima Sidjilani,[e] Abdelkader Bentayeb,[f] Friha Khelfaoui,[f] Nawal Belmiloud,[g] Sid Ahmed Bendella,[a] Lakhdar Alagui,[h] Anis Samy Amine Dib,[a] and Mohammed Noureddine Belkaid[a]

The full-potential linearized augmented plane wave (FP-LAPW) method within the framework of density functional theory (DFT) and semi-classical Boltzmann transport theory under the constant relaxation time approximation has been employed to investigate the structural, mechanical, optoelectronic and thermoelectric properties of novel half-Heusler (HH) ZrYAu alloys (where Y = B or Al) with a valence electron count (VEC) of 8. Our results indicate that both compounds are mechanically stable in structure Type 1 and possess negative formation energies. Additionally, ZrBAu and ZrAlAu display semiconducting behavior, with ZrBAu showing a direct band gap, 0.753 eV (0.774 eV) at point Γ→X and ZrAlAu exhibiting an indirect band gap, 0.431 eV (0.482 eV) at point Γ→Γ, using the generalized gradient approximation (GGA) and Modified Becke and Johnson-generalized gradient approximation (mBJ-GGA), respectively. Based on optical properties, both ZrBAu and ZrAlAu exhibit high optical conductivity within the visible spectrum. In terms of visible light absorption, ZrBAu primarily absorbs blue light, while ZrAlAu absorbs yellow, blue-green and violet light. However, both compounds are effective absorbers of UV light. Regarding thermoelectric performance, the thermoelectric parameters reveal that ZrBAu and ZrAlAu demonstrate significant p-type thermoelectric power. These half-Heusler alloys have a high-power factor, making them promising candidates for thermoelectric applications.

1. Introduction

Due to their exceptional capacity to regulate electrical conductivity, the semiconductor materials are essential available to development of contemporary technology. Their key role in the production of integrated circuits, solar cells, transistors and diodes, among other electronic and optoelectronic components, accounts for their prominence.[1,2] Semiconductors are the key to power electronics for increasing conversion and electric motor efficiency while lowering losses.[3,4] Enhancing solar panels and energy storage system performance is a form of renewable energy.[5] Large-scale data processing and sophisticated computations are made easier by information and communication technologies, which also enable faster processors and higher-density memory.[6] Electronic implants and diagnostic equipment have advanced as a result of medical devices.[7] Flexible display technologies and advancement of light-emitting diode (LED) and organic light-emitting diode (OLED) screen quality are examples of display technologies.[8] Naturally, moving from silicon[9] and binary semiconductors[10] to more intricate ternary[11] or multinary materials[12] greatly expands the range of possible compounds. Over the last few years, half-Heusler compounds – a type of ternary intermetallics – have attracted a lot of attention because of their promise in a variety of industrial applications.[13,14] Due to the unusual way in which these compounds have half-metallic,[15]

[a] R. N. El Imene Bennoui, W. Adli, F. Belkharroubi, S. A. Bendella, A. S. A. Dib, M. N. Belkaid
Laboratory of Analysis and Application of Radiations (LAAR), Department of Engineering Physics, Faculty of Physics, University of Science and Technology of Oran Mohamed Boudiaf (USTO-MB) 1505 El Menouar 31000, Oran, Algeria

[b] Y. Al-Douri
College of Health and Medical Techniques, Al-Bayan University, Baghdad, Iraq
E-mail: yaldouri@yahoo.com

[c] Y. Al-Douri
Department of Mechanical Engineering, Faculty of Engineering, Piri Reis University, EflatunSk, No. 8, 34940 Tuzla, Istanbul, Turkey

[d] Y. Al-Douri
Nanotechnology and Catalysis Research Centre, University of Malaya, 50603 Kuala Lumpur, Malaysia

[e] F. Sidjilani
Laboratoire de Physique des Plasmas, Matériaux Conducteurs et leurs Applications (LPPMCA), Université des Sciences et de la Technologie d'Oran Mohamed Boudiaf, USTO-MB, BP1505, El M'naouar, Oran, Algeria

[f] A. Bentayeb, F. Khelfaoui
Laboratory of physicochemical studies, University of Saida-Dr. Moulay Tahar,Saïda, Saida 20000, Algeria

[g] N. Belmiloud
Departement de Génie Physique, Laboratoire LPMF, Université des Sciences et de la Technologie d'Oran, Mohamed Boudiaf, Oran, Algeria.

[h] L. Alagui
Laboratoire de ressources, matériaux et écosystèmes, Faculté des sciences de bizerte, Université de Carthage, Tunisie

semiconducting,[16–20] and insulating[21–23] properties, a great deal of study has been done to better understand and utilize these properties for real-world applications. There are two types of semiconductors HH compounds, also known "closed-shell compounds," which are classified into two categories according to their valence electron counts (VEC), which range from 18 to 8. HH compounds with VEC = 18 belong to the first category, where Z is a p-element and X and Y are usually transition metals.[24] The I-I-VI, I-II-V, I-III-IV, II-II-IV and II-III-III are the different configurations the elements X, Y and Z take on the second category of HH compounds, which have a VEC = 8. The Roman numerals in these arrangements correspond to valence electrons of elements X, Y and Z in that order. In this case, the elements Y and Z that are the most electronegative, receive n valence electrons from the most electropositive element, X.[25]

Numerous theoretical research has focused on HH compounds with a VEC = 8. Ciftci et al.[26] In their study of I-III-IV HH compounds, have compared the electrical, thermoelectric and structural characteristics with various conduction valences. They highlighted the variations caused by the absence of filled d-levels and emphasized the great thermoelectric potential of KScX (X = C and Ge) compounds. Ahmad et al.[27] have used computational methods within the framework of density functional theory (DFT) to analyze half-Heusler alloys XMgN (X = Li, Na, and K). They have examined these materials' electrical, thermoelectric and structural characteristics. The findings showed that KMgN has an indirect band gap, while LiMgN and NaMgN have direct band gaps. According to Hoat et al.,[28] RbYSn is a half-Heusler (HH) compound belonging to I-III-IV group with a VEC of 8. It has characteristics that make it a good candidate for thermoelectric applications. For RbYSn, large thermopower values are produced by the flatness of the valence band and an appropriate band gap. While, Azouaoui et al.[29] have studied the LiCaX (X = N, P, and As) half-Heusler semiconductors. Their study has revealed that all the compounds are semiconductors with indirect band gaps that decrease when P and As are substituted for N. But Toual et al.[30] have investigated the electrical, thermoelectric, structural and thermo-elastic stability characteristics of LiYN (Y = Mg and Ca) half-Heusler compounds using first-principles computational techniques. They have discovered that these compounds behave like semiconductors and structurally stable in the α-LiYN phase. And, Miri et al.[31] have used DFT-based WIEN2k code to investigate the pressure effect on the optoelectronic and structural properties of LiYP (Y = Ca, Mg, and Zn) half-Heusler semiconductors. Density functional theory (DFT) is employed by Wafula et al.[32] to investigate the thermal, optical, electrical, elastic and structural characteristics of YSiAu, YGeAu and YSnAu half-Heusler alloys. They have discovered that these compounds are anisotropic, ductile and stable both dynamically and mechanically. Khandy et al.[33] have utilized DFT and Boltzmann transport theory to study the structural, electrical, elastic, and thermoelectric properties of CuLiS and CuLiTe half-Heusler alloys. They have found that these alloys have semiconducting properties and stable chemically and energetically. Otherside, Rasul et al.[34] have used sophisticated simulation tools to investigate the structural, electronic, phonon, optoelectronic and physiomechanical properties of LiXBe (X = N, P) half-Heusler compounds. While, Bahara et al.[35] have utilized WIEN2k to study half-Heusler compounds of SrCaGe and SrCaSn. With direct bandgaps, 0.78 eV for SrCaGe and 0.52 eV for SrCaSn, the study showed that both materials are semiconducting, ductile and mechanically stable.

In this work, we carry out systematic calculations using the FP-LAPW method[36] to research the structural stability and optoelectronic properties of two 8-electron HH compounds from the $X^{I}Y^{III}Z^{IV}$ category: (ZrYAu, Y = B, Al). We will demonstrate the distinctive thermoelectric and optoelectronic potential of ZrYAu (Y = B, Al) Half-Heusler (HH) compounds. The following for work's primary steps is:

(i) Optoelectronic Potential: For each chemical, ZrYAu (Y = B, Al), the investigation establishes the electronic bandgap and whether it is direct or indirect. In order to evaluate how each compound behaves when it interacts with electromagnetic waves, a number of optical properties is also examined, including the dielectric function, refractive index, absorption coefficient and reflectivity. These evaluations offer a thorough comprehension of materials' optoelectronic response, emphasizing its potential for certain optoelectronic device applications.

(ii) Thermoelectric Performance: We examined ZrYAu compounds' Seebeck coefficients, power factors and thermal conductivity, among other thermoelectric characteristics. We can determine whether our compounds are suitable for thermoelectric applications by evaluating the ZT figure of merit.

Since these compounds have not been studied, our results will be compared to those obtained for other half-Heusler with VEC = 8. The structure of the work is as follows: Section 2 describes the computational methods used in this work. While, section 3 presents the elaborated results concerning structural properties, total energy curves, and structural, optoelectronic and thermoelectric parameters. And section 4 outlines the conclusions.

Computational

With the general formula $X^{I}Y^{III}Z^{IV}$, our half-Heusler (HH) compounds comprise, in particular, the combinations ZrYAu (Y = B, Al). In this case, Z^{IV} stands for Zr, Y^{III} for Y, and X^{I} for Au. The various Wyckoff positions in the half-Heusler composition that the three atoms, X, Y, and Z, can occupy are given in Table 1.

Density Functional Theory (DFT)[37] is a powerful computational method for studying the electronic structure of materials, with applications ranging from material science to quantum chemistry.[38- 45] The structural, elastic, optical and electronic properties of half Heusler (HH) ZrYAu (Y = B, Al) compounds with a face-centered cubic (FCC) structure are calculated using the Full-Potential Linearized Augmented Plane Wave (FP-LAPW) method within the framework of Density Functional Theory (DFT), as implemented in WIEN2k package.[46] To obtain consistent results for the electronic properties, the exchange and correlation (EX) potential is treated using Perdew-Burke-Ernzerhof generalized gradient approximation (GGA-PBE).[47] Alternatively, the (EX) potential is addressed using the modified Becke-Johnson potential

Table 1. Wycoff positions for the three atoms X, Y and Z in cubic type structure for half Heusler.

	4 a (X)	4 b (Y)	4 c (Z)
Type I	(1/4, 1/4, 1/4)	(0,0,0)	(1/2, 1/2, 1/2)
Type II	(0,0,0)	(1/2, 1/2, 1/2)	(1/4, 1/4, 1/4)
Type III	(1/2, 1/2, 1/2)	(1/4, 1/4, 1/4)	(0,0,0)

scheme (*mBJ*-GGA).[48,49] There will be four steps in the resolution process: (i) figuring out how stable the structure is; (ii) assessing its electronic properties; (iii) solving the Kramers-Kronig equation[50–51] to find optical properties; (iv) using the Boltzmann transport relation[52] to compute thermoelectric properties. The unit cell in FP-LAPW method is split into two regions: The interstitial space is the area that sits between the nucleus and valence states. The accuracy and efficiency of DFT calculations rely on the appropriate selection of various numerical parameters, such as the maximum quantum number and plane wave cutoff energy. A collection of non-overlapping spheres centered on each atom and RMT radius are known as a muffin tin radius sphere. The convergence parameters, which are taken to have a value of $RMT \times K_{max} = 8$, govern the size of basis sets composed of plane waves. Here, RMT stands for the smallest atomic sphere radius, while K_{max} is the magnitude of biggest K vector in the plane wave expansion.

In the present work, the optimal selection of these parameters for a specific system is investigated, where the limit on the growth of spherical harmonics inside atomic spheres and plane waves in the interstitial regions is set to a maximum quantum number, $l_{max} = 10$. To ensure consistency, the plane wave cutoff energy, G_{max}, is set to 12. To preserve a distinct difference between the valence and core states, a cutoff energy of −6 Ryd is chosen. The values for charge and energy convergence are 10^{-3} and 10^{-5} Ryd, respectively. The integration is applied in the reciprocal space using a mesh of 12×12×12, yielding 2000 k-points in the irreducible zone of Brillouin (IBZ),[53] which is adequate to attain convergence. We have chosen muffin-tin (MT) radii, 2.31, 1.8, 1.9 and 2.5 a.u. for Zr, B, Al and Au in that order. The BoltzTraP code[54] in WIEN2k is to calculate the thermoelectric characteristics. Based on the semi-classical Boltzmann transport equation, the BoltzTraP code makes using of constant relaxation time approximation (CRTA).[55] The computation of all thermoelectric properties is done taking into account temperatures between 300 and 1200 K. Each element has the following electronic configuration:

$Z_r \equiv [K_r]\ 4d^2 5s^2$, $B \equiv [He]\ 2s^2 2p^1$ $Al \equiv [Ne] 3s^2 3p^1$, and $Au \equiv [X_e] 4f^{14} 5d^{10} 6s^1$

2. Results and Discussion

2.1. Structural Optimization and Formation Energy

2.1.1. Structural Optimization

To determine the equilibrium parameter and understand how total energy fluctuates depending on this parameter, the total energy of HH ZrYAu (Y = B, Al) compounds in the non-magnetic state (NM) is optimized. The structural optimization is achieved by minimizing total energy as a function of volume V. The optimization cycle is repeated until the point at which convergence is threatened. The Murnaghan's equation od state provided by[56] is used to adjust the curve of variation of total energy in relation to the volume obtained at the end of cycle to evaluate the compression module to equilibrium.

$$E(V) = E_0 + \frac{9\,V_0 B_0}{16}\left\{\left[\left(\frac{V_0}{V}\right)^{2/3} - 1\right]^3 B'_0 + \left[\left(\frac{V_0}{V}\right)^{2/3} - 1\right]^2 \times \left[6 - 4\left(\frac{V_0}{V}\right)^{2/3}\right]\right\} \quad (1)$$

This represents the fundamental as the minimal energy, denoted as E_0, Bulk modulus (B_0) and derivative Bulk modulus (B_0'). When a material is in its fundamental state, its parameter a_0 is matched by volume known as V_0. The relationship between total energy and volume, which is used to evaluate the two compounds' structural stability, is shown in Figure 1. Among the three designs, cubic type I has the lowest energy, as the graph also shows.

The bulk modulus (B) in GPa, its derivative (B′), optimized equilibrium lattice constant (a_0) in Å, and total energy (E_{tot}) per formula unit in Ryd are summarized in Table 2. Since the structure type I for both compounds show a lower energy than other structural types, the evidence supports the idea that the compounds are more stable in this configuration. The computed equilibrium lattice constants in cubic type I structure for half-Heusler (HH) ZrBAu and ZrAlAu compounds are 5.771 Å and 6.332 Å, respectively. The accuracy of our calculations is confirmed by the fact that lattice parameter computed for HH ZrBAu and HH ZrAlAu compounds is pretty close to the theoretical values.[25] A minimal energy of −45343.927142 Ry for ZrBAu and −45780.060035 Ry for ZrAlAu is indicated by our data for the structure type I. The corresponding bulk modulus values are 118.64 GPa and 146.60 GPa, respectively. For the chemical elements from B to Al, an upward correlation is seen between the lattice characteristics and atomic number (Z). In contrast, when the atomic number rises, bulk modulus falls.

2.1.2. Formation Energy

The formation energy (E_f) shows the chemical stability of compound, and is defined by the following equation:[57–58]

$$E_f = E_{XYZ}^{total} - \left[E_X^{bulk} + E_Y^{bulk} + E_Z^{bulk}\right] \quad (2)$$

where E_{XYZ}^{total} is total energy in cubic structure with configuration type I and E_X^{bulk}, E_Y^{bulk}, E_Z^{bulk} are energy of each atom in its standard state. Our calculations yielded formation energies, −0.66 eV for ZrBAu and −2.38 eV for ZrAlAu, as presented in Table 2. Based

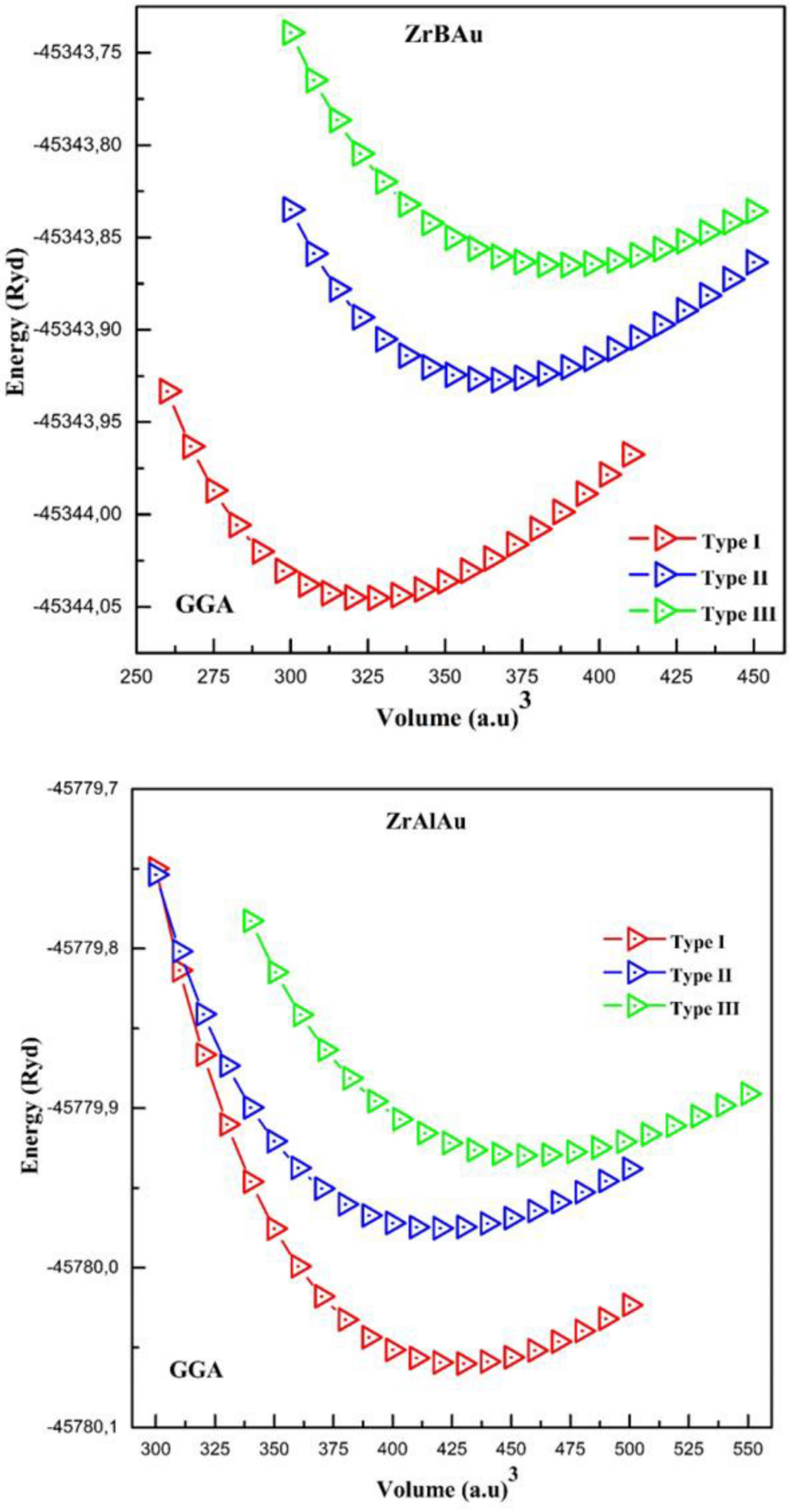

Figure 1. Total energy as a function of volume for three types of cubic structure for HH ZrYAu (Y = B, Al) compounds using GGA.

Table 2. The calculated equilibrium lattice constant (a_0) in Å, bulk modulus (B) in GPa and its derivatives (B′); the total energies (E_{tot}) per formula unit (in Ryd) and formation energy (in Ry) for ZrYAu (Y = B, Al) half Heusler in comparison with other theoretical results.

Compound		Structure	a (Å)	B	B′	E_{min}	E_{form}
ZrBAu	Our work	Type I	5.771	146.60	4.88	−45343.927142	−0.66
		Type II	6.009	159.06	4.51	−45344.045309	
		Type III	6.127	113.53	4.61	−45343.864990	
	Other study		5.774[1]	–	–	–	
ZrAlAu	Our work	Type I	6.332	118.64	4.41	−45780.060035	−2.38
		Type II	6.289	97.70	4.56	−45779.975298	
		Type III	6.471	82.72	4.30	−45779.929668	
	Other study		6.311[1]	–	–	–	

[1]Ref: [25]

on these negative energy values, it appears that these chemicals are experimentally produced and thermodynamically stable. We suggest that our results be used as a guide for further research in this field in the event that experimental or theoretical data are not readily available for comparison.

2.2. Elastic Properties

Using the technique created by Thomas CHARPIN and included in WIEN2k package, we are able to calculate the elastic constants from total energy.[59] Understanding the energy curve as a function of lattice deformation is necessary to calculate elastic constants. The elastic behavior of a material is determined by its tensor C_{ij}. We just require the three parts of half-Heusler compounds: C_{11}, C_{12}, and C_{44}, because we have a cubic structure.[60–62] Consequently, to calculate them, a set of three equations is required. The bulk modulus B that is calculated in the first equation, is connected to the elastic constants by the following:

$$B = \frac{C_{11} + 2C_{12}}{3} \tag{3}$$

The second equation uses the following statement to compute C_{11}-C_{12} by using a tetragonal stress tensor with volume conservation:[59,62]

$$\overline{\delta} = \begin{pmatrix} \delta & 0 & 0 \\ 0 & -\delta & 0 \\ 0 & 0 & \delta^2/(1-\delta^2) \end{pmatrix} \tag{4}$$

The applied stress is represented by δ. The total energy from its unstressed value is impacted by the application of this stress in the following:

$$E(\delta) = E(-\delta) = E(0) + (C_{11} - C_{12})V\delta^2 + O[\delta^4] \tag{5}$$

where V_0 is volume of undeformed unit cell and E(0) is energy of crystal without stress. Lastly, we apply the following expression to compute C_{44} using a tetragonal stress tensor with volume conservation:

$$\overline{\delta} = \begin{pmatrix} 0 & 1/2\delta & 0 \\ 1/2\delta & 0 & 0 \\ 0 & 0 & \delta^2/(4-\delta^2) \end{pmatrix} \tag{6}$$

The changes affect the energy, which is given by the formula:

$$E(\delta) = E(-\delta) = E(0) + 1/2C_{44}V\delta^2 + O[\delta^4] \tag{7}$$

Combining equations (5) and (6) makes it easy to find the two elastic constants, C_{11} and C_{12}; additionally, equation (7) itself can be utilized to quickly obtain the third elastic constant, C_{44}. The Born-Huang stability criterion[62–63] mentioned in eq. (8) must be followed by materials that are mechanically stable.

$$C_{11} - C_{12} > 0\, C_{11} > 0\, C_{44} > 0\, C_{11} + 2C_{12} > 0 \text{ and } C_{12} < B < C_{11} \tag{8}$$

The computed values presented in Table 3 confirm that the elastic constants′ positivity and compliance with the requirements. Our knowledge of the literature indicates that HH ZrYAu (Y=B, Al) elastic characteristics are not covered by any experimental or theoretical evidence. Therefore, it can be said that the calculated elastic constants provided may provide insightful information to the body of existing research.

The shear modulus G, Young's modulus E, anisotropic factor (A), bulk modulus (B), Cauchy pressure CP and Poisson's ratio σ, all are commonly measured for polycrystalline materials, and calculated using the elastic constants. The correlations between these mechanical attributes and elastic constants are commonly expressed as follows:

The Cauchy pressure[64] is given by:

$$CP = C_{12} - C_{44}, \tag{9}$$

Table 3. The ZrYAu (for Y = B, Al) compounds' calculated values for elastic constants Cij, bulk modulus B, shear modulus G (GPa), Young's modulus E, bulk modulus to shear modulus ratio B/G ratio, Poisson's ratio σ, Zener anisotropy factor A, Cauchy pressure CP, sound velocity (transverse vt, longitudinal vl, and average sound vm) in ms^{-1}, Debye temperature θ_D (K), and Grünstein coefficient γ.

	ZrBAu	ZrAlAu
C_{11}	228.19	173.48
C_{12}	101.23	90.54
C_{44}	98.13	88.61
B	143.55	118.19
CP	3.1	1.93
E	165.97	111.39
G	82.41	65.33
σ	0.31	0.34
A	1.56	2.14
B/G	1.75	1.81
v_t	2125.91	2814.95
v_l	4646.77	4990.01
v_m	2395.92	3131.29
θ_D	271.784	337.055
γ	2.285	1.602

The Zener anisotropy factor (A) is expressed by the relation[65–67]

$$A = \frac{2C_{44}}{C_{11} - C_{12}} \tag{10}$$

The Shear Modulus,[68–70] is defined using the following relation:

$$G = \frac{G_R + G_V}{2} \tag{11}$$

where G_R is Reuss shear modulus and G_V is Voigt shear modulus.[68–70] Here is how G_V and G_R are expressed:

$$G_V = \frac{C_{11} - C_{12} + 3C_{44}}{5} \tag{12}$$

$$G_R = \frac{5(C_{11} - C_{12})C_{44}}{4C_{44} + 3(C_{11} - C_{12})} \tag{13}$$

The Poisson's ratio σ[69] is defined by:

$$\sigma = \frac{C_{12}}{C_{11} + C_{12}} \tag{14}$$

The modulus of Young Tensile[70] is given by the following:

$$E = \frac{(C_{11} - C_{12})(C_{11} + 2C_{12})}{C_{11} + C_{12}} \tag{15}$$

Table 3 provides the values of B/G ratio, shear modulus (G), Poisson's ratio (σ), anisotropy factor (A) and Young's modulus (E) for ZrYAu (Y = B, Al) half-Heusler compounds, offering key insights into their mechanical properties. The bulk modulus evaluates the capacity of material to endure pressure-induced volume compression. According to the bulk modulus value, 143.55 GPa for HH ZrBAu and 118.19 GPa for HH ZrAlAu, a correlation of bulk/shear moduli (B/G) proposed by Pugh[71–73] can be used to evaluate ductility. The resistance to fracture is represented by bulk modulus B and resistance to plastic deformation that is shown by shear modulus G. Pugh's criteria states that a material is considered ductile if its B/G ratio is greater than 1.75; if not, it is considered brittle. The calculated B/G value of HH ZrBAu is 1.75 and 1.81 for HH ZrAlAu, demonstrating their ductility. The bottom and upper bounds of σ in solids for ionic crystals and central forces are reported as 0.25 and 0.5, respectively.[74] Also, these values range from 0.1 to 0.25 for covalent materials and non-central forces. We find that HH ZrBAu has a Poisson's ratio σ value, 0.31 and 0.34 for HH ZrAlAu, highlighting the material's major ionic bonding and interatomic forces are central. The Poisson's ratio σ can be used to assess whether a material is brittle or ductile. If this alloy's critical value is less than 0.26, it is considered brittle. At higher values, it exhibits ductile behavior. discover that Poisson's ratio σ value, 0.31 for HH ZrBAu and 0.34 for HH ZrAlAu indicates ductile behavior. The Cauchy pressure CP is another indicator of brittleness or ductility. Based on our findings, our alloys exhibit a positive value, 3.1 GPa for ZrBAu and 1.93 GPa for ZrAlAu, indicating ductile behavior. An understanding of material's overall mechanical behavior and its ability to tolerate deformation can be gained from the computed Young's modulus E, which is helpful in circumstances when a precise balance between stiffness and flexibility is essential. The measured values are 165.97 GPa and 111.39 GPa for ZrBAu and ZrAlAu respectively. ZrBAu is more stiffness than ZrAlAu. A Perfect isotropy is represented by a Zener anisotropy factor (A) of 1, while values that are either below or above one implies anisotropy.[75] As can be seen from Table 3, both HH ZrBAu and ZrAlAu show anisotropic behavior with 1.56 and 2.14 for ZrBAu and ZrAlAu, respectively.

The Debye temperature[49] plays a crucial role in studying the transport phenomena of ZrBAu and ZrAlAu compounds. It is directly related to average velocity v_m through the following:[76–77]

$$\theta_D = \frac{h}{k_B}\left[\frac{3n}{4\pi}\left(\frac{N_A\rho}{M}\right)\right]^{1/3} v_m \tag{16}$$

The symbols h stands for Planck constant, k_B for Boltzmann constant, N_A for Avogadro's number, ρ for material density, M for molecular mass and n for number of atoms. Comprehending the relationship between the average sound velocity v_m, longitudinal v_l and transverse v_t velocities is fundamental for understanding the mechanical and thermodynamic properties of materials. This connection provides a standardized method for determining θ_D and emphasizes the relationship between elastic wave quality and fundamental thermodynamic parame-

ters. The transverse and longitudinal sound velocities, v_t and v_l, respectively are required to calculate the average sound velocity v_m.[63–64]

$$v_m = \left[\frac{1}{3}\left(\frac{2}{v_t^3} + \frac{1}{v_l^3}\right)\right]^{-1/3} \quad (17)$$

$$v_l = \sqrt{\frac{3B + 4G}{3\rho}} \quad (18)$$

and

$$v_t = \sqrt{\frac{G}{\rho}} \quad (19)$$

Table 3 displays the computed v_m, v_t and v_l sound velocities as well as θ_D. To our knowledge, there is not a literature on these characteristics for this specific alloy; nevertheless, further experimental studies will confirm our calculated results.

2.3. Electronic Properties

2.3.1. Band Structure

Our electronic band structure (BS) graph, which we produced using GGA[45] with a black solid line and with *mBJ*-GGA[46–47] in red dash line approximation, is displayed in Figure 2. The Fermi level is configured to be at 0 eV. HH ZrBAu's calculated band structure reveals an indirect band gap Γ-X, where the conduction band minimum (CBM) forms at point X and valence band maximum (VBM) forms at point Γ. Nevertheless, the ZrAlAu (BS) has a direct band gap (X–X), with the VBM and CBM lying at point X. Table 4 presents the computed energy band gap values using GGA and *mBJ*-GGA. The following values are recorded, 0.753 eV (0.774 eV) for ZrBAu and 0.431 eV (0.482 eV) for ZrAlAu with GGA (*mBJ*-GGA). The expansion of band gap is observed to be correlated with atomic number Z of chemical element Y, where Y = B, Al.

Table 4. The band gap energies Eg values and nature of the gap for HH ZrYAu (Y = B, Al) in with GGA and *mBJ*-GGA. All energies are in eV.

Alloy	Study	Eg (eV)	gap	Nature of gap
ZrBAu	GGA	0.753	X→Γ	Indirect
	mBJ- GGA	0.774	X→Γ	Indirect
ZrAlAu	GGA	0.431	X→X	Direct
	mBJ- GGA	0.482	X→X	Direct

In conclusion, the two chemicals demonstrate distinct forms of bandgaps; ZrBAu possesses an indirect bandgap (Γ-X) whereas ZrAlAu exhibits a direct bandgap (X–X). Near the valence band maximum (VBM), the electronic band structure shows a correlation between the heavy and light bands. When it comes to ZrBAu, the VBM is at point Γ, while for ZrAlAu, it is at point X. One of the most important variables in semiconductor transport processes is the effective mass (m*) of charge carriers; electrons (m_e^*) and holes (m_h^*). In fact, whether a carrier's effective mass is higher or lower, it directly affects their ability to migrate. Additionally, the Seebeck coefficient and electrical conductivity are closely related; for example, the Seebeck coefficient rises with the same effective mass while electrical conductivity falls. The effective hole mass (m_h^*) at valence band maximum (VBM) and effective electron mass (m_e^*) at conduction band minimum (CBM) for ZrBAu and ZrAlAu alloys that are calculated using:

$$m^* = \hbar^2 \left(\frac{d^2E}{dk^2}\right)^{-1} \quad (20)$$

where $\hbar$ is reduced Planck constant and continuous function *E(k)* is derived by fitting the energies *E* at band edges *k* to a parabolic function.[76–77] Table 5 displays that the electron effective mass (m_e^*) at conduction band lowest is less than hole effective mass (m_h^*) at valence band maximum. The p-type ZrBAu and p-type ZrAlAu may exhibit the highest Seebeck coefficient indicating significant thermoelectric potential.

2.3.2. Density of States

To fully understand the electronic band structure of half-Heusler alloys in this work, their total (TDOS) and partial density (PDOS) states are also presented. The TDOS plots for the two compounds are shown in Figure 3 using GGA and *mBJ*-GGA. The overall profile of TDOS is similar to the two compounds. We noted that in the neighborhood of CBM and VBM, the curves are almost identical for both compounds and approximations.

The PDOS are shown in Figure 4 using *mBJ*-GGA. For the two compounds, the overall characteristics of PDOS are comparable. For the ZrBAu curve (Figure 4), a small peak is

Table 5. Effective masses of the irreducible Brillouin zone's electrons (m_e^*) and holes (m_h^*)) at various symmetry positions.

ZrBAu		ZrAlAu	
m* (Γ-X) (electron)	2.38	m* (Γ-X) (electron)	1.82
m* (X–W) (electron)	0.727	m* (W-X) (electron)	0.666
m* (Γ-X) (light hole)	1.30	m* (W-X) (light hole)	0.348
m* (Γ-X) (heavy hole)	1.44	m* (W-X) (heavy hole)	1.22
m* (Γ-L) (hole light)	2.36	m* (Γ-X) (light hole)	1.31
m* (Γ-L) (hole heavy)	2.55	m* (Γ-X) (heavy hole)	1.43

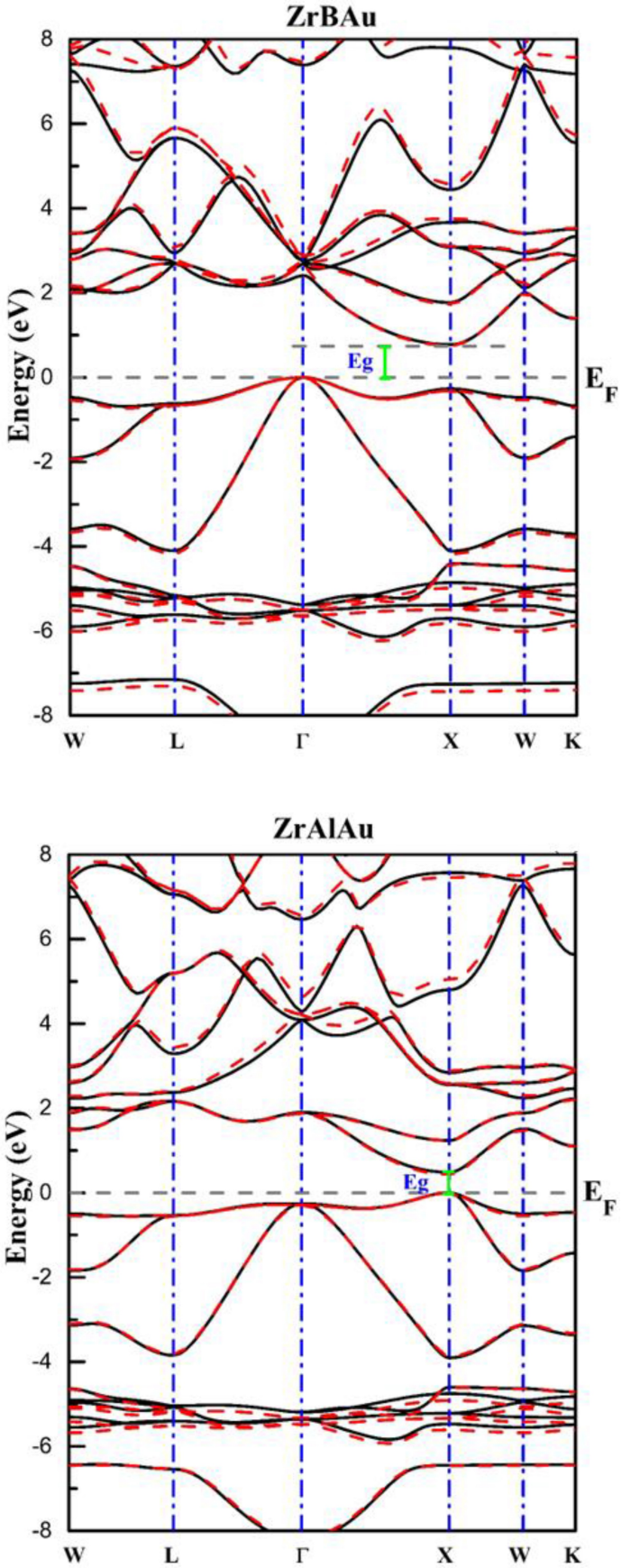

Figure 2. Band structures of the HH ZrYAu (Y = B, Al) compounds with GGA (solid black line) and *mBJ*-GGA (dash red line) at its equilibrium lattice constant.

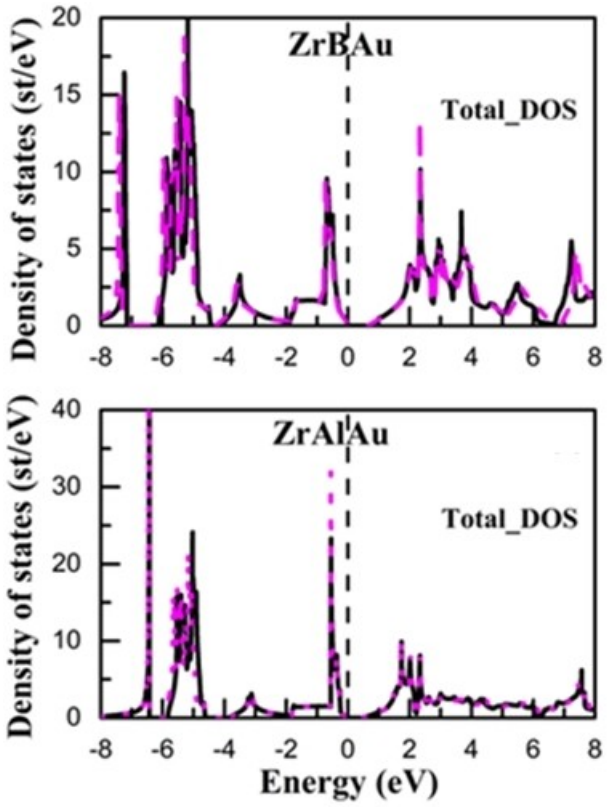

Figure 3. Total density of states (TDOS) of the HH ZrYAu (Y = B, Al) compounds with a GGA (solid black line) and *mBJ*-GGA (dash magenta line) at their equilibrium lattice constant.

detected at energy point, −7.23 eV due to a hybridization between the states 4d-Zr, 2 s-B and 6 s-Au in the valence region and at places far from Fermi level. Many similar peaks appear in the interval between −6.21 eV and −4.77 eV. These peaks are a result of hybridization between the states 2p-B, 6 s-Au and 4d-Zr. Between −4.6 eV and −0.33 eV, this region is occupied by 2 s-B, 2p-B and 6 s-Au states.

The two regions situated within the interval from −7.05 eV to −6.12 eV and interval from −4.39 eV to −4.06 eV are unoccupied. The valence band situated near-Fermi level, where hybridization occurs between the 2p-B, and 4d-Zr states. In the conductance band, the CBM is occupied by 2p-B states, with a dominance of 4d-Zr states. Many sharp peaks are found between 1.77 eV and 4.06 eV, primarily occupied by 4d-Zr states and representing hybridization between the 2 s-B, 2p-B and 5 s-Au states. Four states: 2 s-B, 2p-B, 4d-Zr and 6 s-Au are found in the high-energy range until 8 eV. Regarding the ZrAlAu curve (Figure 4), in the valence a steep peak is detected at a very low energy point, precisely at −6.35 eV, which can be attributed to 4 s-Al, d-Zr and 6 s-Au states. There is nothing present between −6.54 eV and −5.98 eV. The area between −5.93 eV and −4.58 eV is occupied by many sharp peaks due to 3 s-Al, 4d-Zr and 6 s-Au states. The area between −4.57 eV and −4.11 eV is unoccupied. States of 3 s-Al, 3p-Al, 4d-Zr and 5 s-Au are observed in the region between −4.11 eV and Fermi level. The sharp peak that appears at −0.52 eV is due to hybridization between 3p-Al and 4d-Zr states. The VBM is primarily formed by 3p-Al and 4d-Zr states. In the conduction region, the CBM is occupied by 3p-Al states, with a dominance of 4d-Zr states. For positions within the energy interval, 2.07 eV to 8 eV, the 4d-Zr states are mostly occupied, while the 3 s-Al, 3p-Al and 6 s-Au states are also presented. In the interval between 1.12 eV and 3.5 eV, several peaks appear, with the sharpest detected at 1.68 eV. This region is mainly occupied by 3p-Al states and predominantly by 4d-Zr states. At higher energies, the conduction band is occupied by 3 s-Al, 3p-Al and 6 s-Au states, with a dominant presence of 4d-Zr states.

2.4. Optical Properties

The optical characteristics allow one to describe their response to electromagnetic radiation and comprehend their nature. These characteristics are closely associated with electronic transitions between occupied and unoccupied states. An excellent understanding of the materials' optical nature can be gained from studying their use in optoelectronic devices.

Complex Dielectric Function ε(ω): This function explains a material's reaction to an electromagnetic field by taking into account both the material's real and imagined energy storage and dissipation capacities. It is essential for comprehending how materials behave optically and electrically.

The complex differential equation ε(ω) determines the material's response in the electromagnetic field and consists of two parts: $\varepsilon(\omega)=\varepsilon_1(\omega)+i\varepsilon_2(\omega)$. The imaginary portion $\varepsilon_2(\omega)$ describes the material's absorption behavior and is related to the electronic band structure as follows:[48,49,78–83]

$$\varepsilon_2(\omega)=\frac{4\pi^2e^2}{m^2\omega^2}\sum_{ij}\int||\langle i|M|j\rangle|^2f_i(1-f_i)|\times \delta(E_f-E_i-\hbar\omega)d^3k \quad (21)$$

where M is dipole matrix, i and j are the initial and final states, respectively, fi is Fermi distribution function for state i, Ei is electron's energy in state i with a wave vector k, and ω denotes the incident frequency of wave. The real part $\varepsilon_1(\omega)$ of electrical function provides information about the material's polarizability and can be computed from the imaginary part using Kramers-Kronig relations:[48,49,76–80]

$$\varepsilon_1(\omega)=1+\frac{2}{\pi}\int_0^\infty\frac{\omega'\varepsilon_2(\omega')}{\omega'^2-\omega^2}d\omega' \quad (22)$$

The two contributions to dielectric function are intra-band transitions, which describe the transitions that occur within the band of conduction or valence, and inter-band transitions, which describe the transitions between the bands of valence and conduction. The optical properties of HH ZrBAu and HH ZrAlAu are calculated using *ab initio* method implemented in WIEN2k code using the correlation of exchange method (*mBJ*-

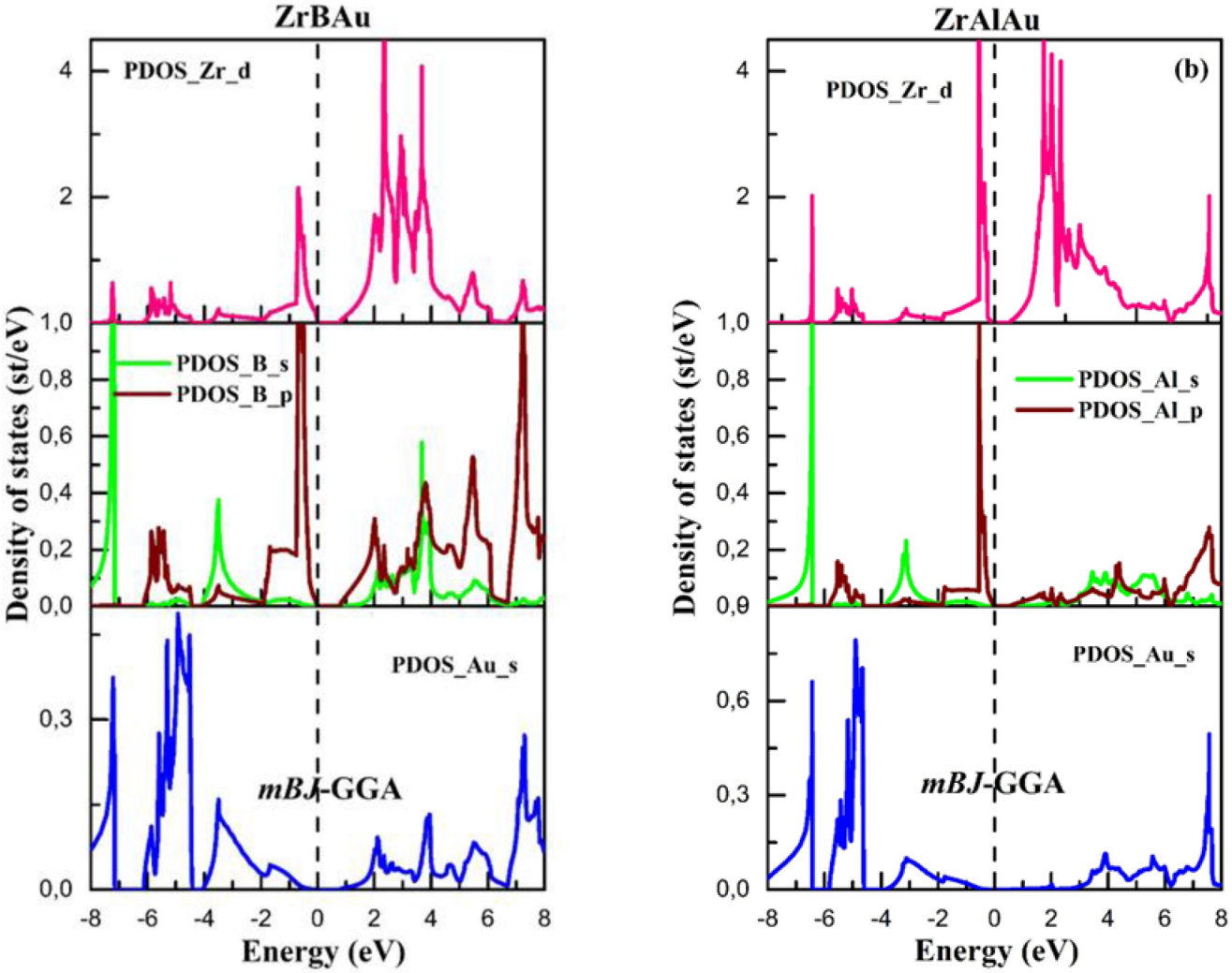

Figure 4. Total and partial density of states of the HH ZrYAu (Y = B, Al) compounds with a *mBJ*-GGA at its equilibrium lattice constant.

GGA) for the cubic structure. This work is conducted for a wide range of energies (0–20 eV).

2.4.1. Imaginary Part of DF

Within Figure 5(a), an orange line shows the spectra $\varepsilon_2(\omega)$ of ZrYAu (Y = B, Al) for a cubic structure as a function of photon energy. The threshold energy, also known as critical point of optical absorption boundary, is produced at 1.09 eV (1140 nm in IR spectrum) for ZrBAu and 0.52 eV (2390 nm in IR spectrum) for ZrAlAu. The absorption region is created by electronic optical transitions between the valence and conduction bands. ZrBAu exhibits strong absorption in energy range, 1.72 eV to 8.16 eV: corresponding to wavelengths from 721 nm to 152 nm, and ZrAlAu in range, 1.33 eV to 5.42 eV: corresponds to wavelengths from 932 nm to 229 nm. The absorption range spans from the visible to ultraviolet (UV) spectrum for ZrBAu and from IR to UV spectrum for ZrAlAu. Significant phonon absorption is seen at energies that match a number of peaks. For every compounds, we have chosen five peaks with the labels E_1, E_2,… E_5, and determined the various energies, related wavelengths and spectral range for ZrYAu (Y = B, Al), all results are listed in Table 6. Based on the acquired results, it is discovered that HH ZrBAu and HH ZrAlAu exhibit inter-band transitions in two different light spectrum domains: UV and visible. It can be observed that $\varepsilon_2(\omega)$ reaches zero at energies over 14.5 eV for ZrBAu and above 13 eV for ZrAlAu, suggesting that these compounds turn transparent at these energies. In the studies conducted by Belkilali et al.,[17] the NaScSi compound exhibits multiple transition peaks spanning from the infrared (IR) to the ultraviolet (UV) range. However, Azzi et al.[18] have found that the two KZnN and KZnP compounds, display their transition peaks within the UV region. In summary, it is observed that transitions between the valence band (VB) and conduction band (CB) are more significant in the visible range for HH ZrAlAu and in UV for the two compounds.

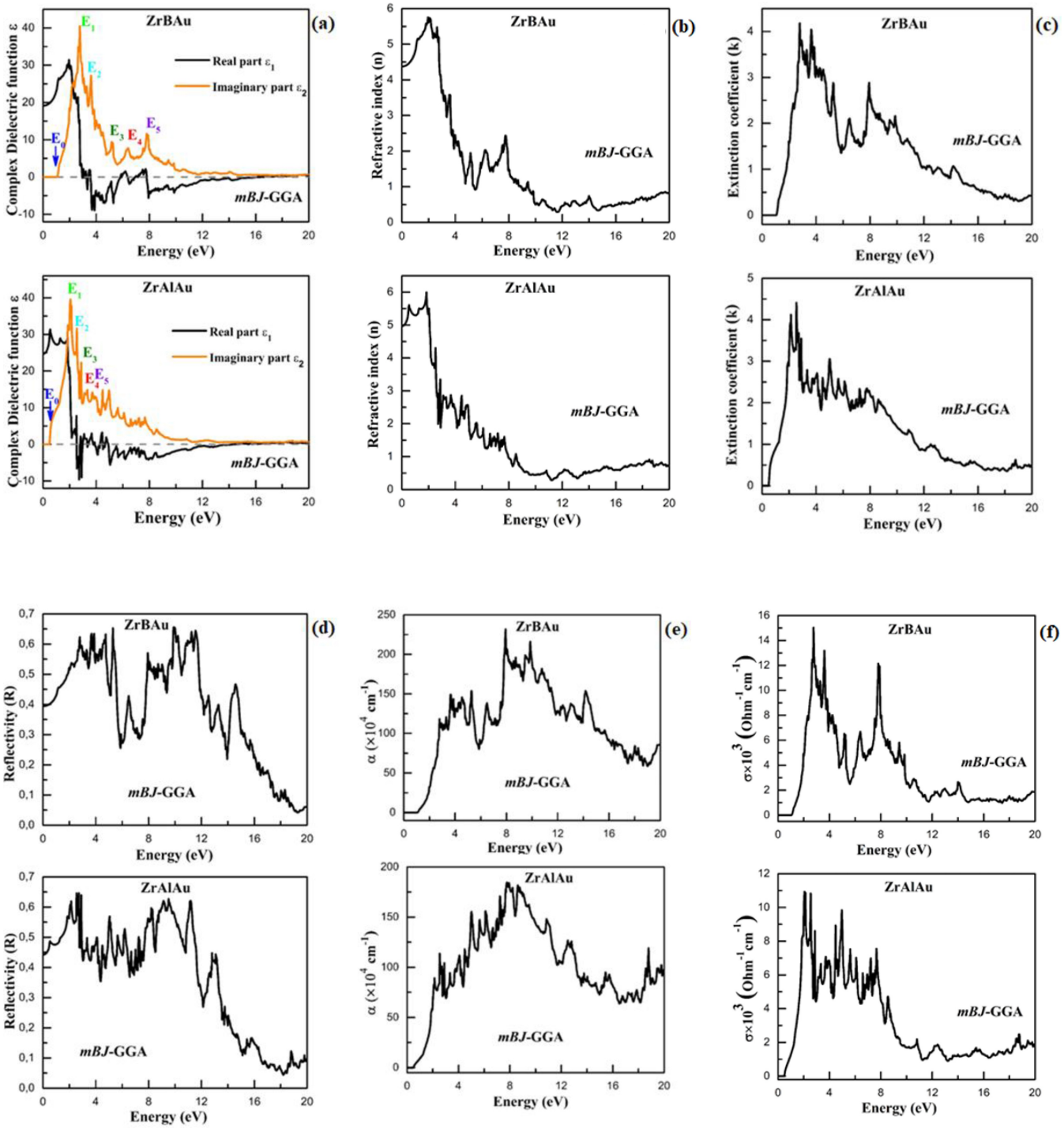

Figure 5. (a) Complex dielectric function ε(ω), (b) Refractive index n(ω), (c) extinction coefficient k (ω), (d) reflectivity coefficient R(ω), (e) absorption coefficient α(ω) and (f) Optical conductivity σ(ω) of HH ZrYAu (Y = B, Al) compounds versus photon energy using *mBJ*-GGA.

2.4.2. The Real Part of DF

The real components of DF $\varepsilon_1(\omega)$ are shown by the black line in Figure 5(a), ZrBAu and ZrAlAu. For ZrBAu compound, the static value, ε1(ω) at 0 eV is 19.46, while for ZrAlAu complex, it is 24.87, these results are listed in Table 7. From this static value, $\varepsilon_1(\omega)$ increases and reaches its maximum, 30.91 in the visible spectrum (red region) at 1.97 eV (629 nm), then falls and becomes zero in UV spectrum at 2.81 eV (442 nm) for HH ZrBAu in visible spectrum blue light region. When it comes to HH ZrAlAu, the higher peak is 30.92, is found at energy, 0.59 eV (2102 nm in IR region).

The next step $\varepsilon_1(\omega)$ decreases until $\varepsilon_1(\omega) = 0$ at 2.53 eV of energy (490 nm) in the visible spectrum (blue-green region). $\varepsilon_1(\omega)$ turns negative upon cancellation: for HH ZrBAu, this happens between 3.59 eV and 16.53 eV, while for HH ZrAlAu, it

Table 6. The main transitions E_{v-c}, energy (eV), wavelength (nm), and spectrum for ZrYAu (Y = B, Al) compounds with *mBJ*-GGA.

E_{v-c}	ZrBAu			ZrAlAu		
	Energy	Wavelength +	Spectrum	Energy	Wavelength	Spectrum
E1	2.78	446	Visible (Blue)	2.06	602	Visible (Red-Orange)
E2	3.64	341	UV	2.53	490	Visible (Blue-Green)
E3	5.23	237	UV	2.87	432	Visible (Violet)
E4	6.38	194	UV	3.26	380	Near UV
E5	7.87	158	UV	4.46	278	UV

Table 7. Static values of: real part of dielectric function $\varepsilon 1(0)$, refractive index $n(0)$ and reflectivity $R(0)$ for ZrYAu (Y = B, Al) with *mBJ*-GGA.

Alloy	ε1(0)	n(0)	R(0)
ZrBAu	19.27	4.39	39.67 %
ZrAlAu	24.87	4.99	44.70 %
KSrSb	6.4[1]	–	–
KSrBi	6.1[1]	–	–
KZnN	9.152[2]	3.025[2]	68 %[2]
KZnP	8.379[2]	2.895[2]	51 %[2]
CaMgC	7.93[3]	–	–
CaMgSi	10.59[3]	–	–
CaMgGe	11.30[3]	–	–
CaMgSn	12.52[3]	–	–
CaMgPb	13.68[3]	–	–
CaCuP		2.91[4]	65.70 %[4]
CaAgP		2.81[4]	64.94 %[4]

[1]Ref: [76]; [2]Ref: [18]; [3]Ref: [19]; [4]Ref: [16].

happens between 3.35 eV and 14.75 eV. These lower values of $\varepsilon_1(\omega)$ correspond to higher reflectivity values for ZrBAu and ZrAlAu, respectively as illustrated in Figure 5(d). ε1(ω) stabilizes when the energy of HH ZrBAu and HH ZrAlAu surpasses 16.77 eV and 16.49 eV, respectively, and this indicates that there is a little interaction between the incident photons and material. According to Azzi et al.,[18] the limit values of $\varepsilon_1(0)$ obtained for KZnN and KZnP compounds are 9.152 and 8.379, respectively. On the other hand, Saim et al.[19] have observed ε1(0) values, 7.93 for CaMgC, 10.59 for CaMgSi, 11.30 for CaMgGe, 12.52 for CaMgSn, and 13.68 for CaMgPb. The limit values of ε1(0) for the ZrBAu and ZrAlAu are the highest among those reported. Knowing $\varepsilon_1(\omega)$ and $\varepsilon_2(\omega)$ allows for the calculation of other optical characteristics, such as the absorption coefficient α (ω), refractive index n(ω), reflectivity R(ω) and optical conductivity σ(ω).[81–86]

$$n(\omega) = \left(\frac{\sqrt{\boldsymbol{\varepsilon}_1^2(\boldsymbol{\omega}) + \boldsymbol{\varepsilon}_2^2(\boldsymbol{\omega})} + \boldsymbol{\varepsilon}_1(\boldsymbol{\omega})}{2}\right)^{\frac{1}{2}} \tag{23}$$

$$\mathrm{k}(\omega) = \frac{1}{\sqrt{2}}\left[(\varepsilon_1(\omega)^2 + \varepsilon_2(\omega)^2)^{1/2} - \varepsilon_1(\omega)\right]^{1/2} \tag{24}$$

$$R(\omega) = \left|\frac{\sqrt{\varepsilon(\omega)} - 1}{\sqrt{\varepsilon(\omega)} + 1}\right|^2 \tag{25}$$

$$\alpha(\omega) = \frac{\sqrt{2}\omega}{\mathrm{c}}\left[\left(\varepsilon_1^2(\omega) + \varepsilon_2^2(\omega)\right)^{\frac{1}{2}} - \varepsilon_1(\omega)\right]^{\frac{1}{2}} \tag{26}$$

$$\mathrm{Re}[\sigma(\omega)] = \frac{\omega}{4\pi}\varepsilon_2(\omega) \tag{27}$$

2.4.3. Refractive Index n(ω)

Knowing the physical parameter that quantifies the attenuation and phase velocity of electromagnetic waves in a material is important. According to accepted theory, the curve n(ω) (Figure 5(b)) strongly resembles the $\varepsilon_1(\boldsymbol{\omega})$ spectrum. Index of static refractiveness n(0): 4.39 for ZrBAu and 4.97 for ZrAlAu. The formula $n(0) = \sqrt{\varepsilon_1(0)}$ can be used to find n(0) at ω = 0. Table 7 lists the values of the static refractive index n(0). From ZrBAu curve, at 1.96 eV (633 nm) in the visible spectrum (red region), the refractive index achieves a maximum value of 5.71. However, it falls within the energy ranges of 2.73 eV–4.65 eV (454 nm–267 nm), which extends from the visible to UV

spectrum. For the energy equals 8.69 eV, $n(\omega)$ takes the value, 1. From energies greater than 8.69 eV (143 nm), which corresponds to UV spectrum, n(ω) becomes less than 1. Regarding ZrAlAu curve, the static value is n(0) = 4.99. The highest values of n(ω) are 5.60 at 0.52 eV (2390 nm) in IR spectrum and 6.02 at 1.81 eV (686 nm), which is in the visible spectrum of red-light region. The rapid decreasing of n(ω) occurs in the range of 2.00 eV (619 nm) to 2.92 eV (425 nm), which belongs to the visible domain, spanning from the orange-red region to blue-violet region. For the energy equals 7.97 eV, n(ω) takes the value, 1. The energies for refractive indices less than 1 are greater than 7.97 eV (156 nm), which is in UV domain. According to Azzi et al.,[18] the static refractive index at a frequency of 0, n(0) is 3.025 for KZnN and 2.895 for KZnP. However, the values reported by Drici et al.[16] are 2.91 for CaCuP and 2.81 for CaAgP. When comparing these results, we observe that n(0) for both ZrBAu and ZrAlAu compounds is higher.

2.4.4. The Extinction Coefficient $k(\omega)$

The extinction coefficient k(ω), shown in Figure 5(c), reaches a maximum value, 4.78 at energy, 2.81 eV for ZrBAu alloy, and a maximum value, 4.40 at energy, 2.53 eV for ZrAlAu alloy. These results align with the energies that nullify the real parts of dielectric function, as $\varepsilon_1(2.81) = 0$ for ZrBAu and ε_1 (2.53) = 0 for ZrAlAu.

2.4.5. Optical Reflectivity R(ω)

The ratio of energy of incident wave to the reflected wave is known as optical reflectivity, or R(ω). ZrBAu and ZrAlAu's R(ω) spectra are shown in Figure 5(d), and the static reflectance R(0) for the two compounds is listed in Table 7. We can see that ZrBAu has a static reflectance R(0) of 39.67% at nearly zero frequency. The reflectivity is then found to be at its highest in two separate locations. The energy intervals corresponding to the first and second regions are 1.90 eV to 5.61 eV and 7.78 eV to 11.87 eV, respectively. Maximum reflectivity values of 62.6% at 2.78 eV (446.3 nm), 63.2% at 3.73 eV (332.63), 64.9% at 4.75 eV (261.2 nm) and 64.9% at 5.28 eV (234.98 nm) are seen in the first region. Maximum reflectivity is found in the second interval at 9.9 eV (125.32 nm), 11.29 eV (109.89 nm) and 11.54 eV (107.51 nm), with corresponding values, 65.1%, 64.26% and 64.48% situated in UV spectrum. From the HH ZrAlAu curve, we notice that the static reflectivity R(0) at almost zero frequency is 44.5%. A broad range where the reflectivity is maximal is located between 1.76 eV and 11.57 eV. A high concentration of reflectivity is detected at 2.78 eV (446.04 nm) with a value, 64.26%, and three peaks with 62.2% at 9.13 eV (135.82 nm), 9.51 eV (130.18 nm) and 11.19 eV (110.81 nm). For both compounds, there are a noticeable decreasing in reflectivity values at higher energies.

According to Azzi et al.,[18] the highest reflectivity for KZnN is at 4.08 eV (303.92 nm), reaching 68%, while for KZnP, the peak reflectivity occurs at 3.99 eV (310.78 nm) with a maximum of 51%. So, for Drici et al.,[16] the most intense peak for CaCuP compound is at 5.86 eV (212.01 nm), with a maximum reflectivity, 65.70%, and for CaAgP compound, the peak is at 4.73 eV (262.66 nm) with a maximum reflectivity, 64.94%. From these results, it is evident that KZnN exhibits maximum reflectivity in UV range, while KZnP shows significant reflectivity in the same region. In contrast, the energy values for CaCuP and CaAgP correspond to the infrared spectrum. Our ZrBAu and ZrAlAu display maximum reflectivity in the visible and UV regions.

2.4.6. The Absorption Coefficient α(ω)

The absorption coefficient is a crucial optical parameter that describes how light intensity changes as it travels through a material. In this context, α(ω) is proportional to the imaginary part of dielectric function. The peaks and troughs in the absorption spectra indicate potential transitions between the valence band and conduction band states. Figure 5(e) presents the absorption curves for ZrBAu and ZrAlAu. This curve reveals two regions of significant absorption of ZrBAu. The first region is situated between the visible and UV spectrum, ranging from 2.73 eV (454.16 nm) to 5.42 eV (228.75 nm). The second region spans the UV spectrum, from 6.18 eV (201.27 nm) to 20 eV (61.88 nm). The peak in the visible region has an intensity, 117.80×10^4 cm^{-1} and is detected at 2.77 eV, corresponding to a wavelength, 447.95 nm, which falls within the blue region of visible spectrum. In the second region, the peak with the highest intensity, valued at 232.67×10^4 cm^{-1}, is observed at 7.93 eV (156.35 nm). A wide absorption range for ZrAlAu begins at 1.92 eV and continues to higher energies. Three peaks with intensities, 91.43×10^4 cm^{-1}, 113.66×10^4 cm^{-1} and 103.14×10^4 cm^{-1} are found in the visible spectrum at the following locations: 2.11 eV (588 nm) in the yellow light region, 2.54 eV (489 nm) in the blue-green light region and 2.88 eV (431 nm) in the violet light region. There are many peaks in UV range, the strongest of which is at 7.83 eV and has an intensity, 183.84×10^4 cm^{-1}. In Table 8, we have listed some main peaks of absorption and their respective spectrum. In conclusion, we can state that our two materials – ZrBAu for blue light and ZrAlAu for yellow, blue-green and violet light – may be employed as effective light absorbers in the visible spectrum based on data collected. Both substances show notable absorption in UV spectrum. The results obtained by Saim et al.[19] indicate that the absorption of CaMgZ (Z = C, Al, Si, Ge, and Sn) compounds is concentrated in UV region. A similar finding is reported by Azzi et al.[18] for KZnZ (Z = N, P) compounds. In contrast, for ZrBAu and ZrAlAu, the absorption is concentrated between the visible and UV regions.

2.4.7. The Optical Conductivity

This refers to a material's capacity to conduct electricity in reaction to an oscillating electric field, typically associated with light. It combines the effects of material's electron mobility and

Table 8. Absorption intensity ($\times 10^4$ cm^{-1}), energy (eV), and wavelength (nm) of the main absorption peaks of ZrYAu (Y = B, Al) compounds with *mBJ*-GGA.

Alloy	α (ω)	Energy (eV)	Wavelength (nm)	Spectrum
ZrBAu	117.11	2.77	447	Visible: Blue light region
	149.85	3.66	339	UV
	153.01	5.24	237	UV
	231.84	7.93	156.35	UV
	216.29	9.86	126	UV
ZrAlAu	89.58	2.11	588	Visible: Yellow light region
	114.31	2.54	489	Visible: Blue-green light region
	104.98	2.88	431	Visible: Violet light region
	152.49	4.64	267	UV
	184.49	7.83	158	UV

interactions with electromagnetic waves to offer information on material's optical properties such as absorption and reflection.

The optical conductivity curves σ(ω) of HH ZrBAu and HH ZrAlAu for the cubic type I structure are displayed in Figure 5(f). The curves span 0 to 20 eV and shows the fluctuation of σ(ω) as a function of photon energy. Three areas have been identified for HH ZrBAu: in the range from 1.01 to 5.52 eV, many peaks are detected, the strongest is found at 2.73 eV (454.2 nm), where the greatest conductivity is 15000 Ohms^{-1}cm^{-1}. In the second interval, which is located between 5.52 eV and 10.19 eV, multiple peaks are located, the strongest one is positioned at 7.78 eV, where the greatest conductivity is 12176.2 Ohms^{-1}cm^{-1}. The third zone spans greater energies up to 20 eV, beginning at 10.19 eV, optical conductivity in this area remains constant at 1200 Ohms^{-1}cm^{-1}.

The HH ZrAlAu curve exhibits two separate sections: the first region spans from 0.474 eV to 10.09 eV and has many peaks. The strongest peak, which has an intensity of 10967.2 Ohms^{-1}cm^{-1}, is found at 2.11 eV (587.68 nm). The fluctuation becomes nearly constant at 1290 Ohms^{-1}cm^{-1} between 10.09 eV and 20 eV. According to the results obtained by Azzi et al.,[18] the conductivity of KZnN and KZnP is significant in UV region. On the other hand, a study conducted by Drici et al.[16] found that CaCuP and CaAgP exhibit high optical conductivity in UV range. In breif, we can state that the ZrBAu and ZrAlAu have maximal optical conductivities in the visible range, which extend into the UV range.

2.5. Thermoelectric Properties

The increasing recognition of significance of thermoelectric technology in converting waste heat into useable electricity highlights its pertinence in energy management and sustainable practices, as well as its extensive array of applications across various industries. Semi-classical Boltzmann theory is employed for the evaluation of thermoelectric characteristics of ZrYAu alloys (where Y represents B and Al), including parameters such as power factor (*PF*), thermal conductivity (κ), electrical conductivity (σ) and Seebeck coefficient (S). In this study, the implementation of rigid band approximation in BoltzTraP code is employed.[54] We have already anticipated that the chemicals we investigated are semiconductor materials. By utilising the semi-classical Boltzmann transport equations:[89–93]

$$\sigma_{\alpha,\beta}(T,\mu) = \frac{1}{\Omega}\int \sigma_{\alpha,\beta}(\varepsilon)\left[-\frac{\partial f_\mu(T,\varepsilon)}{\partial \varepsilon}\right]d\varepsilon \tag{28}$$

$$S_{\alpha,\beta}(T,\mu) = \frac{1}{eT\Omega\sigma_{\alpha,\beta}(T,\mu)}\int \sigma_{\alpha,\beta}(\varepsilon)(\varepsilon-\mu)\left[-\frac{\partial f_\mu(T,\varepsilon)}{\partial \varepsilon}\right]d\varepsilon \tag{29}$$

$$\kappa_{\alpha,\beta}(T,\mu) = \frac{1}{e^2T\Omega}\int \sigma_{\alpha,\beta}(\varepsilon)(\varepsilon-\mu)^2\left[-\frac{\partial f_\mu(T,\varepsilon)}{\partial \varepsilon}\right]d\varepsilon \tag{30}$$

The variables σ, S, k, μ, (α, β), Ω, e and f_μ correspond to the following: thermal conductivity, chemical potential, electrical conductivity, Seebeck coefficient, tensor indices, unit cell volume, electron charge and Fermi-Dirac distribution function. The underlying premise of this approximation is that the band structure of chemical remains unaltered despite fluctuations in temperature or doping. Within thermoelectric materials, a good candidate is characterized by high efficiency in heat conversion to electricity, a high-power factor (*PF*), high electrical conductivity (σ) and low thermal conductivity (κ). The approach applied in this work only partially accounts for thermal conductivity, which is a combination of lattice vibrations (κ_L) and electronic contributions (κ_e). It is noteworthy that while the Seebeck coefficient (S) is independent of relaxation time (τ), electrical conductivity (σ), thermal conductivity (κ) and power factor (*PF*), all are depended. The study investigates the possibility of using ZrYAu (Y = B, Al) alloys to generate electrical energy from waste heat, providing environmentally friendly energy options for a range of industrial uses. Advanced computational tools are utilized to extensively explore important thermoelectric properties such the Seebeck coefficient, electrical conductivity and thermal conductivity in order to improve these materials' efficiency and performance in energy conversion processes. In this work, we computed these parameters using the *mBJ*-GGA.

2.5.1. Seebeck Coefficient (S)

The Seebeck coefficient (S) is a fundamental parameter used to assess the thermoelectric performance of a material by quantifying the voltage difference produced per unit temperature gradient. The Seebeck coefficient exhibits a clear correlation with the band structure of compounds, hence offering valuable insights into the characteristics of primary charge carriers present in the sample. A positive value of parameter S signifies the presence of p-type conduction, known as hole carriers, whereas a negative value shows the occurrence of n-type conduction, characterized by electron carriers. Figure 6(a) illustrates the variation of Seebeck coefficient for ZrYAu alloys (Y = B and Al) concerning the chemical potential ($\mu - E_F$) within a range of −1.5 eV to 2.0 eV, at different temperatures, 300 K, 600 K and 900 K. In the conduction band, where electrons are the main charge carriers, n-type conduction is indicated by a negative value of S. On the other hand, p-type conduction, which is defined by the majority of carriers being holes in the valence band, is indicated by a positive value of S. These figures clearly show that ZrBAu and ZrAlAu both be defined by the majority of carriers being holes in the valence band, is indicated by a positive value of S. These figures clearly show that ZrBAu and ZrAlAu be like p-type semiconductors. The positive Seebeck coefficient at $\mu - E_F = 0$, which measures 246.03 μV/K for ZrBAu and 260.95 μV/K for ZrAlAu at ambient temperature, lends credence to this result. Two separate peaks can be seen in the region, −1.5 μeV to 2.0 μeV in Figure 6a1 and 6a2. At 300 K, for ZrBAu, these peaks occur at chemical potentials of about 0.331 μeV and 0.453 μeV, and for ZrAlAu, at 0.194 μeV and 0.295 μeV. Because thermal energy increases with temperature, the Seebeck coefficient (S) decreases. The Seebeck coefficient (S) for the two materials under investigation increases gradually, peaking at 300 K, or ambient temperature. The highest documented Seebeck coefficient (S) values for p-type (n-type) conduction at 300 K are 1290.48 μV/K (−1241.27 μV/K) for ZrBAu and 829.66 μV/K (−769.05 μV/K) for ZrAlAu.

Table 9 presents the maximum S values for both compounds at various temperatures. It is observed that Seebeck coefficient decreases as temperature increases. Additionally, the S values for both p-type and n-type conduction in ZrBAu are higher than those in ZrAlAu. According to the findings of Benazouazi et al.,[94] the highest recorded Seebeck coefficient (S) values for both p-type and n-type conduction at 300 K are 1534 μV/K for LiSrN, 1475 μV/K for LiSrP, and 1553 μV/K for LiSrAs. In contrast, Ciftci et al.[26] have reported that the highest Seebeck coefficient values at 300 K are 419 μV/K (−398 μV/K) for KScC and 721 μV/K (−697 μV/K) for KScGe. Meanwhile, Shivastra et al.[92] have noted maximum S values at 300 K for p-type conduction of 920 μV/K for KScSn, 977 μV/K for KScPb, 493 μV/K for KYSi, and 547 μV/K for KYGe. When comparing our results to these previously reported theoretical values, we find that the Seebeck coefficient (S) for ZrBAu at 300 K is higher than that KScC, KScGe, KScSn, KScPb, KYSi and KYGe. For ZrAlAu at 300 K, its Seebeck coefficient is greater than those of KScC and KScGe. However, the Li-based compounds, namely LiSrN, LiSrP and LiSrAs, exhibit the highest maximum S values for both p-type and n-type conduction compared to ZrBAu and ZrAlAu. Behera et al.[76] have found the higher value at 300 K, 2990 μV/K for KSrSb and 2996 μV/K for KSrBi in p-type.

2.5.2. Electrical Conductivity (σ/τ)

The electrical conductivity (σ/τ) is a crucial indicator of a material's ability to conduct electricity. The electronic conductivity (σ/τ) of ZrYAu compounds (Y = B, and Al) as a function of chemical potential ($\mu = \mu\text{-}E_F$) from −1.5 eV to 2.3 eV at temperatures, 300 K, 600 K and 900 K is shown in Figure 6(b), revealing a similar profile. For the ZrYAu compounds (Y = B and Al), electrical conductivity (σ/τ) is higher at a negative chemical potential, suggesting that p-type compositions have superior conductivity compared to n-type ones. This result indicates that hole doping in these compounds is more advantageous for their thermoelectric performance than electron doping. The

Table 9. Maximum values of Seebeck coefficient S(μV K^{-1}); Electric conductivity per relaxation time σ/τ (10^{20} Ω^{-1} m^{-1} s^{-1}); Electric thermal conductivity per relaxation time κ_e/τ (10^{15} W m^{-1} K^{-1} s^{-1}) and power factor per relaxation time *PF* (×10^{11} W K^2 m^{-1} s^{-1}) of ZrYAu (Y = B and Al) half-Heusler.

p-type							n-type				
		S	σ/τ	κ_e/τ	PF	ZT	S	σ/τ	κ_e/τ	PF	ZT
ZrBAu	300	1290.48	4.03	2.91	1.98	0.59	−1241.27	4.01	2.72	1.36	0.53
	600	668.25	3.94	5.57	6.08	0.33	−638.10	3.77	4.87	3.62	0.28
	900	469.84	3.93	7.81	11.20	0.06	−430.16	3.58	6.53	6.47	0.04
ZrAlAu	300	829.66	3.93	2.89	2.97	0.60	−769.05	3.42	2.48	1.04	0.46
	600	457.41	3.88	5.53	7.68	0.36	−410.16	3.33	4.42	2.76	0.25
	900	343.81	3.84	7.80	12.22	0.060	−278.47	3.24	7.80	5.03	0.04
KSrSb	300	2990[(1)]	0.94			≈1	−2785				
	900			1.33		≈1					
KSrBi	300	2996[(1)]	0.96			≈1	−2785				
	900			1.355		≈1					

[1]Ref: [76]

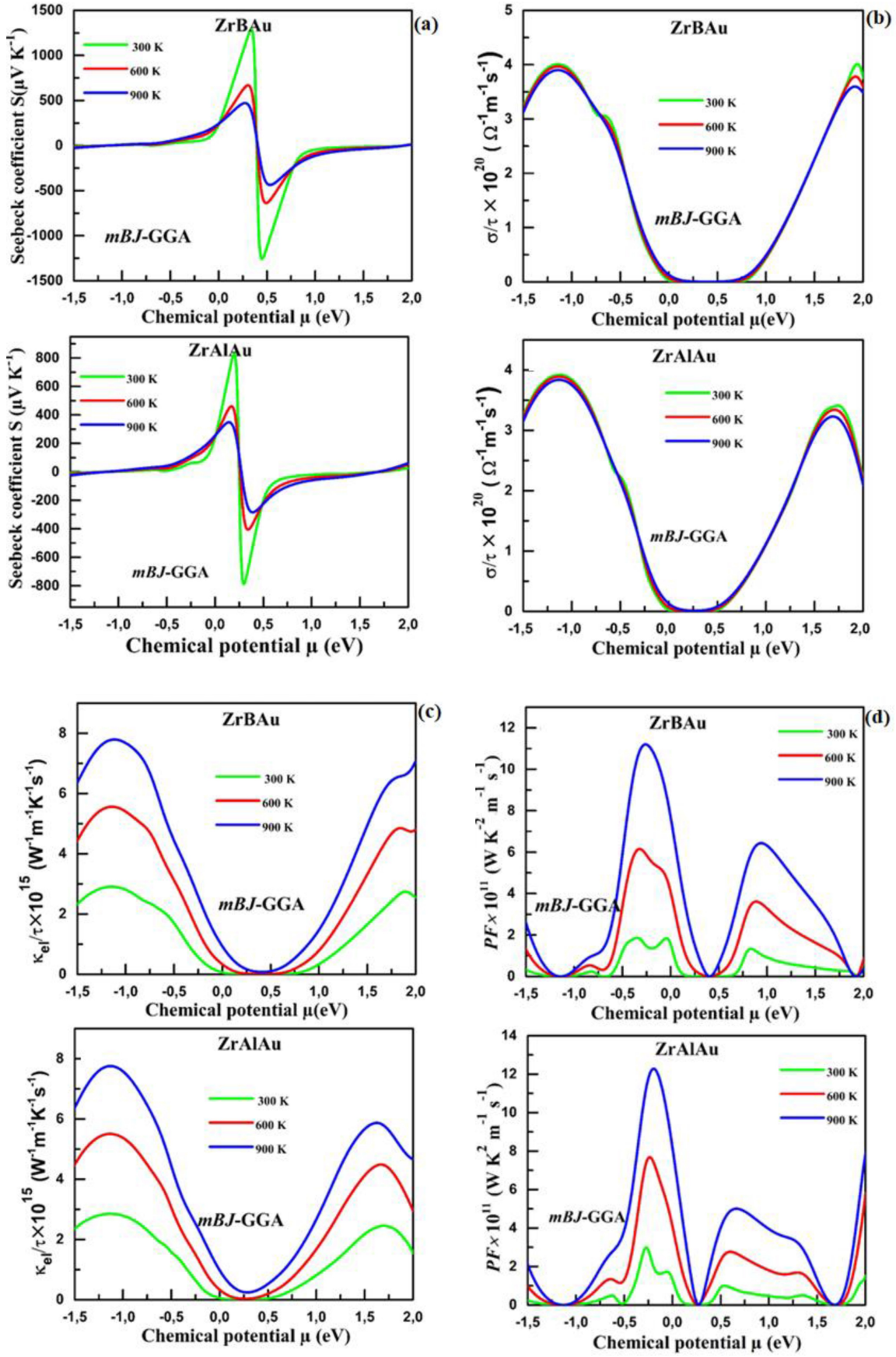

Figure 6. Calculated transport coefficients: (a) Seebeck coefficient (S), (b) Electrical conductivity (σ/τ), (c) Thermal electronic conductivity (κ_{el}/τ), and (d) Power factor (*PF*) as a function of the Chemical potential of the ZrBAu and ZrAlAu at 300 K, 600 K and 900 K.

maximum electrical conductivities σ/τ reach approximately 4.03×10^{20} $(\Omega ms)^{-1}$ and 3.93×10^{20} $(\Omega ms)^{-1}$ at −0.57 eV and −0.58 eV for ZrBAu and ZrAlAu, respectively in p-type region, while in n-type region, they are 4.01×10^{20} $(\Omega ms)^{-1}$ and 3.42×10^{20} $(\Omega ms)^{-1}$ at 1.30 eV and 1.34 eV, respectively. As discussed earlier, the differences in electrical conductivity between ZrBAu and ZrAlAu are attributed to the variations in band gaps and effective masses of these compounds. Remarkably, the computational model indicates that both alloys show an increased electrical conductivity (σ/τ) as temperature rises, suggesting their potential utility in applications requiring stable electrical conductivity over a wide temperature range. Table 9 lists the maximum electrical conductivity values at various temperatures. It is observed that these values decrease as temperature decreases. Moreover, the σ/τ values for p-type (n-type) conduction in ZrBAu are higher than ZrAlAu. According to Benazouazi et al.,[91] the highest documented σ/τ values for p-type (n-type) conduction at 300 K are 15.35×10^{19} $(\Omega ms)^{-1}$ (34.83×10^{19} $(\Omega ms)^{-1}$) for LiSrN, 15.26×10^{19} $(\Omega ms)^{-1}$ (31.33×10^{19} $(\Omega ms)^{-1}$) for LiSrP, and 14.44×10^{19} $(\Omega ms)^{-1}$ (29.91×10^{19} $(\Omega ms)^{-1}$) for LiSrAs. We compared the highest σ/τ values reported by Shrivastava et al.,[92] with our maximum values at room temperature. For KScSn and KScPb, the maximum σ/τ values are approximately 1.62×10^{20} $(\Omega ms)^{-1}$ and 1.66×10^{20} $(\Omega ms)^{-1}$, respectively in p-type region. For KYSi and KYGe, the highest values are 2.02×10^{20} $(\Omega ms)^{-1}$ and 2.04×10^{20} $(\Omega ms)^{-1}$, respectively in n-type region. Additionally, findings by Ciftci et al.[26] have showed that KScC exhibits the highest σ/τ value, 2.71×10^{20} $(\Omega ms)^{-1}$, while KScGe has a value, 1.55×10^{20} $(\Omega ms)^{-1}$ approximately for p-type conduction. Notably, the maximum σ/τ values for our two compounds at room temperature are higher than those reported in previous studies.[26,91,92] As the introduction states, electrical conductivity has not been experimentally studied, and the current findings are in line with earlier computations for these substances.

2.5.3. Electronic Thermal Conductivity

One important metric for assessing a material's capacity to conduct heat is its electronic thermal conductivity (κ/τ). The two main components of thermal conductivity (κ) are the electronic component (κ_e), which results from the movement of heat by electrons and holes and phonon component (κ_L) that is caused by vibrations in the lattice. This paragraph evaluates the electronic thermal conductivity of ZrYAu (Y = B and Al) half-Heusler compounds due to the BoltzTraP code can only calculate the electronic contribution ((κ_e)) to thermal conductivity. The change in electronic thermal conductivity ((κ_e)/τ) at 300 K, 600 K and 900 K as a function of chemical potential ($\mu-E_F$) is shown in Figure 6(c). The data indicates a noteworthy rise in (κ_e)/τ as temperature increases from 300 K to 900 K. Significant similarities exist between electronic conductivity and thermal electronic conductivity profiles. The Wiedemann-Franz law stipulates that (κ_e) = σLT – where L is Lorenz number, σ is electrical conductivity, and T is absolute temperature – is consistent with this discovery. Our results show that the maximal values of (κ_e)/τ at ambient temperature for p-type is 2.89×10^{15} W/mK²s for ZrBAu and 2.97×10^{15} W/mK²s for ZrAlAu at a chemical potential −1.15 eV and −1.14 eV, respectively. The thermal conductivity of ZrBAu and ZrAlAu is virtually zero within the chemical potential ranges of 0.02 eV to 0.77 eV and 0 eV to 0.50 eV, respectively indicating optimal efficiency. For n-type, the maximal values of (κ_e)/τ at ambient temperature is 2.72×10^{15} W/mK²s for ZrBAu and 2.48×10^{15} W/mK²s for ZrAlAu at a chemical potential of 1.89 eV and 1.7 eV, respectively. Thermal conductivity rises dramatically beyond these intervals, especially when temperatures rise from 300 K to 600 K and 900 K. Table 9 presents the maximum (κ_e)/τ values at different temperatures based on chemical potential. It is observed that these values increase with rising temperatures. Additionally, the (κ_e)/τ values for p-type (n-type) conduction for ZrBAu are higher than ZrAlAu.

According to Benazouazi et al.,[91] the highest recorded electronic thermal conductivity ((κ_e)/τ) values at 300 K are 1.08×10^{14} W/mK²s for p-type conduction and 2.51×10^{14} W/mK²s for n-type conduction in LiSrN. For LiSrP, the values are 1.05×10^{14} W/mK²s for p-type and 2.27×10^{14} W/mK²s for n-type. In LiSrAs, the highest values are 1.11×10^{14} W/mK²s for p-type and 2.11×10^{14} W/mK²s for n-type conduction. On the other hand, Ciftci et al.[26] have reported that the maximum (κ_e)/τ values at 300 K for p-type (n-type) conduction are 0.25×10^{14} W/mK²s (0.24×10^{14} W/mK²s) for KScC, and 0.73×10^{14} W/mK²s (0.75×10^{14} W/mK²s) for KScGe. It is noted that at room temperature, the maximum (κ_e)/τ values for both ZrBAu and ZrAlAu are higher than those reported for the compounds mentioned in.[26,91] The findings obtained by Behera et al.[76] have revealed that the higher thermal conductivity given for KSrSb and KSrBi is 1.33×10^{15} W/mK²s and 1.355×10^{15} W/mK²s, respectively for p-type at 900 K.

As mentioned in the introduction, there are no experimental data available on electronic thermal conductivity, and the current results are consistent with previous calculations for these compounds.

2.5.4. Power Factor (PF)

One important statistic for evaluating the efficiency of thermoelectric materials is the Power Factor (*PF*), which is the ratio of real power utilized to apparent power supplied and is defined as $PF = (S^2\sigma/\tau)$. The *PF* measures the efficiency with which these materials transform heat into electricity. The *PF* changes for ZrBAu and ZrAlAu as a function of chemical potential ($\mu = \mu - E_F$) at 300 K, 600 K and 900 K are shown in Figure 6(d). When the chemical potential is halfway between the valence and conduction bands, the electrical conductivity (σ) and Seebeck coefficient (S) are almost zero, which results in *PF* to be zero. One peak for p-type doping and another for n-type doping are visible in *PF*. The maximum *PF* reaches 1.98×10^{11} $W K^2 m^{-1} s^{-1}$ and 2.97×10^{11} $W K^2 m^{-1} s^{-1}$ at −0.05 eV and −0.27 eV for ZrBAu and ZrAlAu, respectively in p-type region, while in n-type region, they are 1.36×10^{11} $W K^2 m^{-1} s^{-1}$ and 1.04×10^{11} $W K^2 m^{-1} s^{-1}$ at 0.85 eV and 0.53 eV, respectively. As

discussed earlier, the differences in electrical conductivity between ZrBAu and ZrAlAu are attributed to the variations in band gaps and effective masses of these compounds. Table 9 lists the maximal *PF* values at various temperatures. It is observed that *PF* values increase as temperature rises. Additionally, the *PF* values for p-type (n-type) conduction in ZrBAu are higher than ZrAlAu. In case of Benazouazi et al.'s study,[91] the highest recorded *PF* values for p-type (n-type) conduction at 300 K are 49×10^{10} $W K^2 m^{-1} s^{-1}$ (14.8×10^{10} $W K^2 m^{-1} s^{-1}$) for LiSrN, 28×10^{10} $W K^2 m^{-1} s^{-1}$ (13.99×10^{10} $W K^2 m^{-1} s^{-1}$) for LiSrP, and 44×10^{10} $W K^2 m^{-11} s^{-11}$ (10.8×10^{10} $W K^2 m^{-1} s^{-1}$) for LiSrAs. With the exception of ZrAlAu's p-type conduction, where its value surpasses that of LiSrP, the maximum *PF* values at 300 K for our two compounds are lower than those of LiSrN, and LiSrAs.

Figure 7 illustrates the variation of *PF* with temperature at a specific chemical potential ($\mu = E_F$). *PF* increases linearly with temperature, reaching its maximum values, 8.84×10^{11} $W m K^2 s$ and 5.58×10^{11} $W m K^2 s$ at 1200 K for ZrBAu and ZrAlAu, respectively. At room temperature, the *PF* values are minimal: 1.55×10^{11} $W K^{-2} m^{-1} s^{-1}$ for ZrBAu and 1.42×10^{11} $W K^{-2} m^{-1} s^{-1}$ for ZrAlAu. According to Shrivastava,[95] the *PF* increases with temperature and reaches its peak values of 8.84×10^{11} $W m K^2 s$, 8.70×10^{11} $W m K^2 s$, 5.34×10^{11} $W m K^2 s$, and 5.58×10^{11} $W m K^2 s$ at 800 K for KScSn, KScPb, KYSi and KYGe, respectively. For our ZrBAu and ZrAlAu, the *PF* values at 800 K are 6.27×10^{11} $W m K^2 s$ and 6.93×10^{11} $W m K^2 s$, respectively. We can confirm that at high temperatures, the *PF* of both ZrBAu and ZrAlAu is greater than KYSi and KYGe. The results of this study align with previous research and could assist experimenters in developing high-temperature thermoelectric materials, particularly for p-type thermo-electrics.

2.5.5. Lattice Thermal Conductivity

For thermoelectric materials to function well, a crystal lattice's thermal conductivity is essential. Julian and Slack have extended and modified Liebfried's original equation to handle complex lattices (with $n > 1$), emphasizing the effect of acoustic vibrations on heat transport. The Slack equation, an empirical formula that may be used to calculate the thermal conductivity of complicated crystal lattices, is developed as a result of this method. The Slack equation can be used to determine the lattice thermal conductivity as referred in [76–77]:

$$\kappa_L = Z(\gamma)\frac{M_a\theta_D^3\delta}{\gamma^2 n^{2/3}}\frac{1}{T} \tag{31}$$

where volume per atom is represented by δ, number of elements per unit cell is denoted by n, Debye temperature is indicated by θ_D, average atomic weight is indicated by M_a and $Z(\gamma)$ coefficient is related to γ (in $W mol/kg m^2 K^3$) as described in reference [82]:

$$A_\gamma(\gamma) = \frac{5.720 \times 0.849 \times 10^7}{1 - \left(\frac{0.514}{\gamma}\right) + \left(\frac{0.228}{\gamma^2}\right)} \tag{32}$$

γ is Grűneisen parameter expressed as follows:

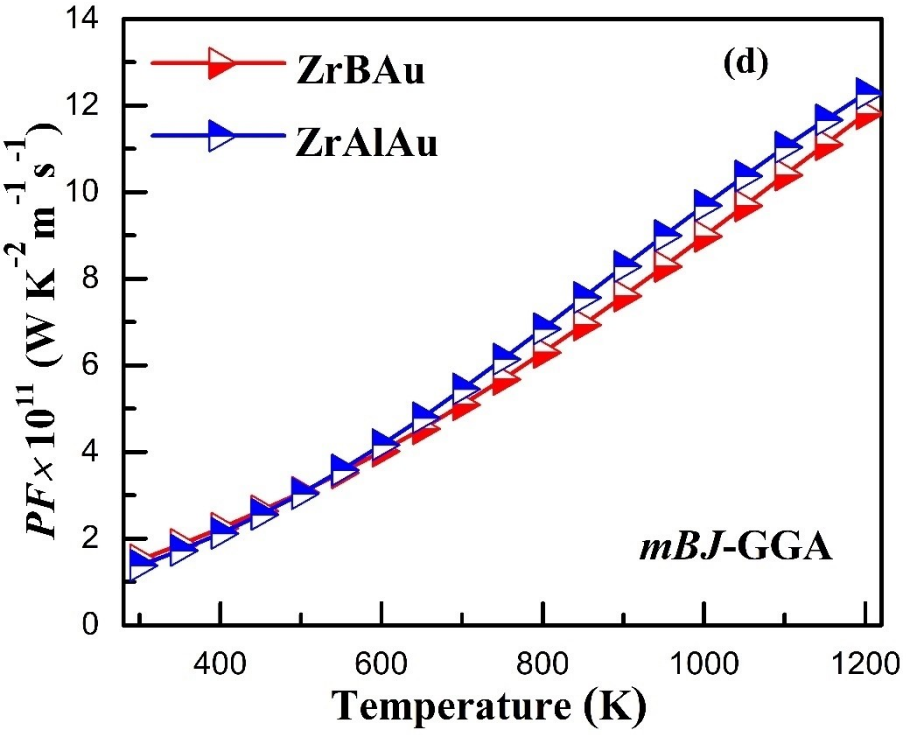

Figure 7. Calculated Power factor (*PF*) as a function of the temperature of the ZrBAu and ZrAlAu ($\mu = E_F$).

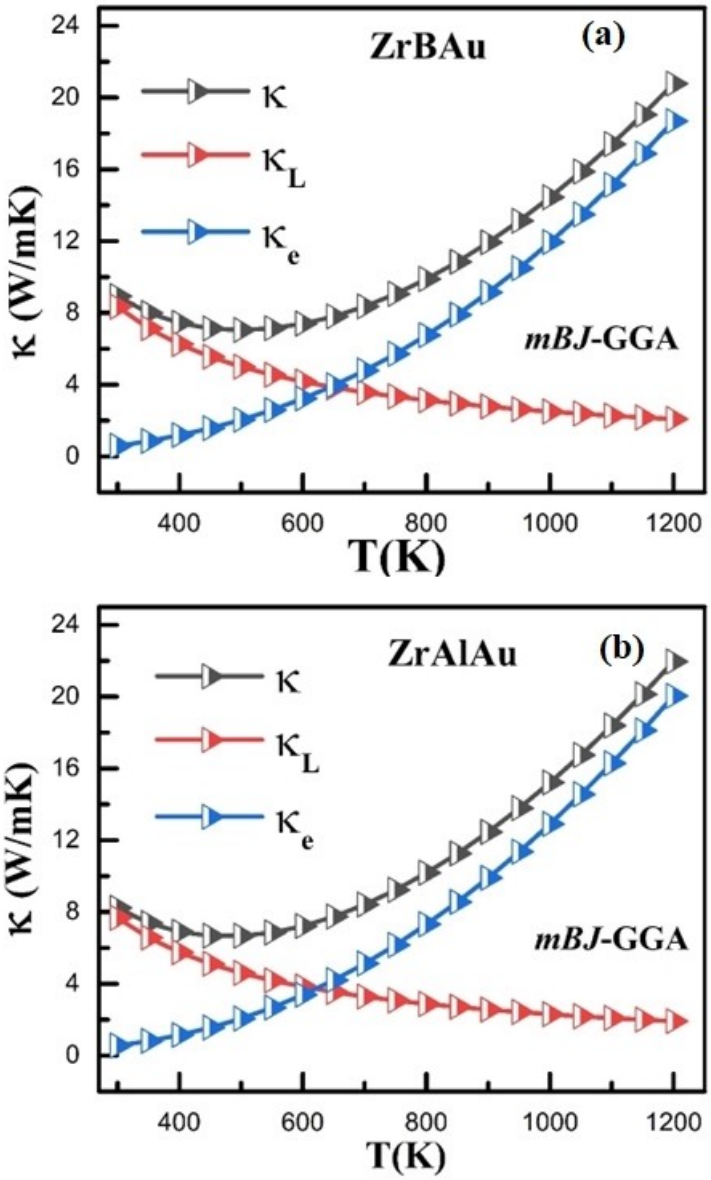

Figure 8. Calculated of Total thermal conductivity (κ), Thermal electronic conductivity (κ_e), and Lattice thermal conductivity (κ_L) as a function of the temperature of (a) ZrBAu and (b) ZrAlAu with *mBJ*-GGA approximation.

$$\gamma = \frac{9 - 12\ (v_t/v_l)^2}{2 + 4\ (v_t/v_l)^2} \tag{33}$$

The Gruneisen parameter, which is related to Debye Temperature, is calculated for ZrBAu and ZrAlAu compounds; the results indicate values, 2.285 and 1.602, respectively as presented in Table 3. The lattice thermal conductivity gradually drops with rising temperature, reaching a maximum at 1200 K as illustrated in Figure 8. This reduction in thermal conductivity has a positive effect on thermoelectric properties of these materials. At room temperature 300 K, ZrBAu and ZrAlAu have respective thermal conductivity (κ_L) values of 8.36 W/m·K and 8.03 W/m·K. while, at 1200 K, these values sharply drop to 2.03 W/m·K for ZrBAu and 1.94 W/m·K for ZrAlAu.

2.5.6. Total Thermal Conductivity

The total thermal conductivity (κ), assuming a default relaxation period of $\tau = 10^{-14}$ s is computed as the sum of electronic thermal conductivity (κ_e) and lattice thermal conductivity (κ_L) in order to maximize the figure of merit ZT. This computation can be expressed by the equation $\kappa = \kappa_e + \kappa_L$. As shown in the Figure 8, the total thermal conductivity (κ) decreases slightly between 300 K and 600 K for both compounds. For ZrBAu, it drops from 9.17 W/m·K to 7.08 W/m·K, while for ZrAlAu, it decreases from 8.36 W/m·K to 6.9 W/m·K. Beyond 600 K, (κ) increases linearly for both compounds, reaching 20.77 W/m·K for ZrBAu and 21.9 W/m·K for ZrAlAu at 1200 K

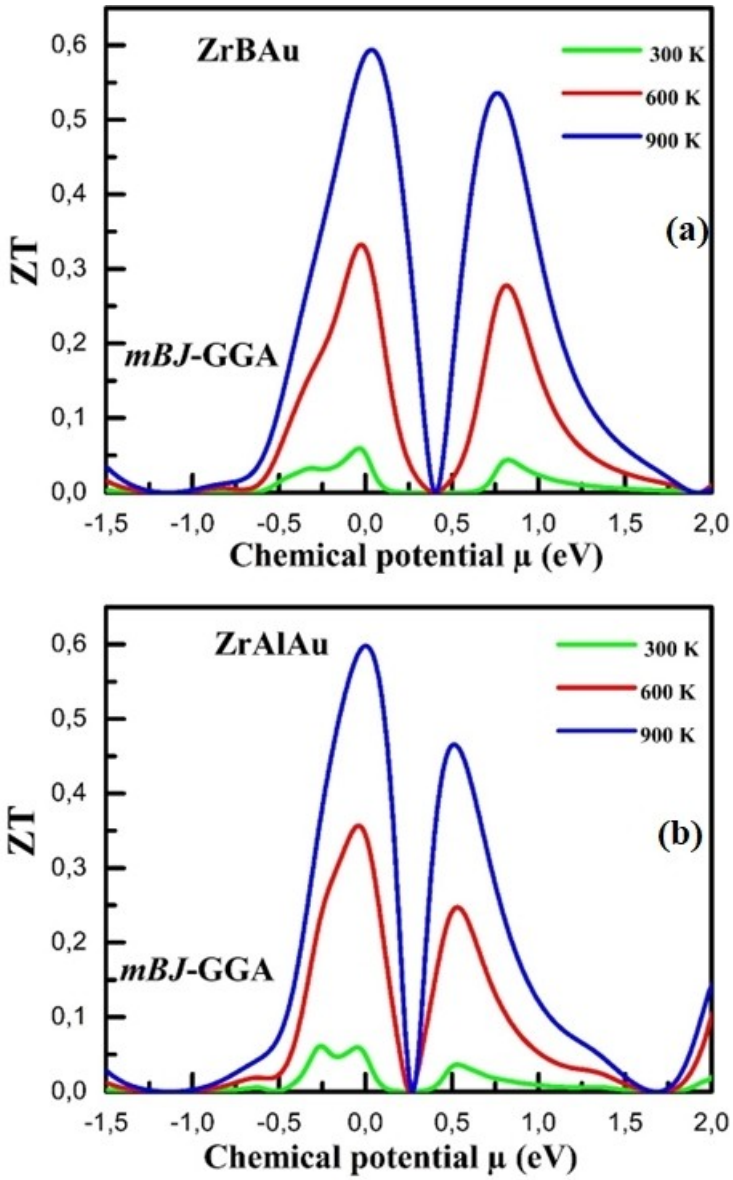

Figure 9. Calculated Figure of merit (ZT) as a function of the chemical potential of (a) ZrBAu and (b) ZrAlAu.

2.5.7. Figure of Merit

The figure of merit (ZT) of thermoelectric material is one of the most crucial parameters for evaluating its efficiency created by setting the default relaxation time to 10^{-14} s. Equation (34), which represents the figure of merit (ZT) (Figure 9), maximizes the power factor while minimizing the overall thermal conductivity.

$$ZT = \frac{S^2 \times \sigma \times T}{\kappa_e + \kappa_L} \tag{34}$$

where S stands for Seebeck coefficient. Where electrical conductivity is denoted by σ, thermal conductivity is denoted by $\kappa = \kappa_e + \kappa_L$ and temperature in absolute terms is T. ZT values for p-type materials at 900 K are 0.59 for ZrBAu and 0.6 for ZrAlAu. On another hand, ZT values for n-type materials are 0.46 for ZrAlAu and 0.53 for ZrBAu. Table 9 contains obtained maximum values of ZT at different temperatures. The results obtained by Behera et al reveal that ZT value is close to unity for KSrSb and KSrBi compounds for p-type.

The figure of merit, ZT, varies with temperature, as seen in Figure 10. For both substances, ZT is found to increase quickly between 300 and 800 K. The Z-T temperature stabilizes at greater temperatures. At 1200 K, the ZrBAu compound reaches a value of 0.68, whereas the ZrAlAu compound has a value of 0.67.

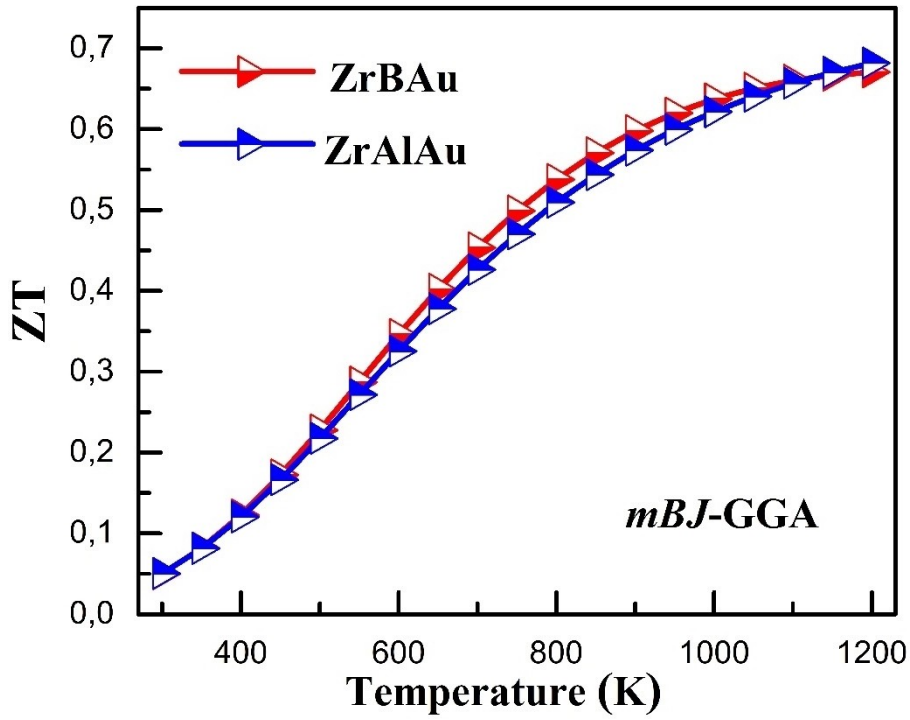

Figure 10. Calculated Total figure merit (ZT) as a function of the temperature of (a) ZrBAu and (b) ZrAlAu ($\mu = E_F$).

3. Conclusions

In this work, we used the FP-LAPW approach in the GGA and *mBJ*-GGA frameworks to theoretically examine the structural, elastic, optoelectronic and thermoelectric properties of ZrYAu (Y = B and Al) half-Heusler compounds. Our structural predictions for ZrYAu compounds are in good agreement with the available theoretical information. The findings suggest that the cubic Type I phase is the most stable state for these chemicals. Furthermore, the bulk modulus drops from B to Al, indicating reduced compressibility, while the lattice parameter rises. We postulated that the half-Heusler ZrYAu (Y = B and Al) compounds exhibit mechanical stability, meeting all the stability requirements for a cubic crystal structure. By employing both GGA and *mBJ*-GGA, the ZrBAu exhibits an indirect band gap ($\Gamma \rightarrow X$), but the ZrAlAu molecule displays a direct band gap ($\Gamma \rightarrow \Gamma$). High reflectivity and characteristic absorption peaks in the visible and ultraviolet (UV) parts of electromagnetic spectrum suggest that these compounds are excellent contenders for application in optoelectronic, photovoltaic and optical devices including ultraviolet (UV) detectors and solar cell systems. An analysis of the thermoelectric characteristics, demonstrates that ZrYAu (Y = B and Al) half-Heusler compounds behave as p-type materials according to *mBJ*-GGA and are promising candidates for thermoelectric applications. We wish that our study will be proved by practical techniques for future experimental works.

Acknowledgements

Y. A. would like to acknowledge Al-Bayan University for fruitful support.

Conflict of Interests

The authors declare no conflict of interest.

Data Availability Statement

All used data is embedded in this manuscript and properly referenced where applicable.

Keywords: FP-LAPW · Half Heusler · Optical · Thermoelectric

[1] N.-K. Nguyen, T. Nguyen, T.-K. Nguyen, S. Yadav, T. Dinh, M. K. Masud, P. Singha, T. N. Do, M. J. Barton, H. T. Ta, *ACS Appl. Electron. Mater.* **2021**, *3*, 1959–1981.
[2] A. Guerrero, J. Bisquert, G. Garcia-Belmonte, *Chem. Rev.* **2021**, *121*, 14430–14484.
[3] Z. Tang, Y. Yang, F. Blaabjerg, *CSEE J. Power Energy Syst.* **2021**, *8*, 39–52.
[4] Y. Zhang, F. Udrea, H. Wang, *Nature electronics* **2022**, *5*, 723–734.
[5] M. Nehra, N. Dilbaghi, G. Marrazza, A. Kaushik, R. Abolhassani, Y. K. Mishra, K. H. Kim, S. Kumar, *Nano Energy* **2020**, *76*, 104991.
[6] N. J. Tye, S. Hofmann, P. Stanley-Marbell, *Nature Electronics* **2023**, *6*, 479–490.
[7] K. Chen, J. Ren, C. Chen, W. Xu, S. Zhang, *Nano Today* **2020**, *35*, 100939.
[8] I. Verboven, W. Deferme, *Prog. Mater. Sci.* **2021**, *118*, 100760.

[9] E. Klugmann-Radziemska, A. Kuczyńska-Łażewska, *Sol. Energy Mater. Sol. Cells* **2020**, *205*, 110259.
[10] M. Tahir, S. Tasleem, B. Tahir, *Int. J. Hydrogen Energy* **2020**, *45*, 15985–16038.
[11] Z. Abbas, K. Fatima, I. Gorczyca, M. Irfan, N. Alotaibi, T. Alshahrani, H. H. Raza, S. Muhammad, *Mater. Sci. Semicond. Process.* **2022**, *146*, 106662.
[12] H. Jin, X. Tan, T. Wang, Y. Yu, Y. Wei, *J. Phys. Chem. Lett.* **2022**, *13*, 7228–7235.
[13] R. Min, Y. Wang, X. Jiang, R. Chen, H. Kang, E. Guo, Z. Chen, X. Yang, T. Wang, *Chem. Eng. J.* **2022**, *449*, 137898.
[14] S. H. Zaferani, R. Ghomashchi, D. Vashaee, *Renewable Sustainable Energy Rev.* **2019**, *112*, 158–169.
[15] L. Feng, E. Liu, W. Zhang, W. Wang, G. Wu, *J. Magn. Magn. Mater.* **2014**, *351*, 92–97.
[16] L. Drici, F. Belkharroubi, F. Z. Boufadi, I. Ameri, M. Ameri, W. Belkilali, S. Azzi, F. Khelfaoui, Y. Al-Douri, *Emergent Mater.* **2022**, *5*, 1–16..
[17] W. Belkilali, F. Belkharroubi, M. Ameri, N. Ramdani, F. Boudahri, F. Khelfaoui, K. Amara, S. Azzi, L. Drici, I. Ameri, *Emergent Mater.* **2021**, *4*, 1465–1477.
[18] S. Azzi, F. Belkharroubi, N. Ramdani, M. Ameri, I. S. Messaoudi, W. Belkilali, L. Drici, L. Blaha, I. Ameri, Y. Al-Douri, A. Bouhemadou, *Rev. Mex. Fis.* **2023**, *69*(1), 060501.
[19] A. Saim, F. Belkharroubi, F. Z. Boufadi, I. Ameri, L. F. Blaha, A. Tebboune, M. N. Belkaid, W. Belkilali, M. Ameri, Y. Al-Douri, A. F. Abd El-Rehim, *J. Electron. Mater.* **2022**, *51*(7), 4014–4028.
[20] F. Belkharroubi, W. Belkilali, F. Khelfaoui, F. Boudahri, M. Zahraoui, N. Belmiloud, K. Bentayeb, E. H. A. Abdellah, R. N. E. I. Bennoui, R. Belbachir, Y. Al-Douri, *Cryst. Res. Technol.* **2024**, *59*(1), 2300238.
[21] X. Wang, X. Dai, H. Jia, L. Wang, X. Liu, Y. Cui, G. Liu, *Phys. Lett. A* **2014**, *378*, 1662–1666.
[22] K. Elphick, W. Frost, M. Samiepour, T. Kubota, K. Takanashi, H. Sukegawa, S. Mitani, A. Hirohata, *Sci. Technol. Adv. Mater.* **2021**, *22*, 235–271.
[23] S. Tavares, K. Yang, M. A. Meyers, *Prog. Mater. Sci.* **2023**, *132*, 101017.
[24] D.-E. Missoum, K. Bencherif, D. Bensaid, *Eur. Phys. J. B* **2023**, *96*, 160.
[25] T. Gruhn, *Phys. Rev. B* **2010**, *82*, 125210.
[26] Y. O. Ciftci, S. D. Mahanti, *J. Appl. Phys.* **2016**, *119*, 145703.
[27] R. Ahmed, N. S. Masuri, B. U. Haq, A. Shaari, S. AlFaifi, F. K. Butt, M. N. Muhamad, M. Ahmed, S. A. Tahir, *Mater. Des.* **2017**, *136*, 196–203.
[28] D. Hoat, M. Naseri, *Chem. Phys.* **2020**, *528*, 110510.
[29] A. Azouaoui, A. Hourmatallah, N. Benzakour, K. Bouslykhane, *J. Solid State Chem.* **2022**, *310*, 123020.
[30] Y. Toual, S. Mouchou, A. Azouaoui, A. Maouhoubi, A. Hourmatallah, N. Benzakour, K. Bouslykhane, *Chem. Phys.* **2023**, *572*, 111967.
[31] M. Miri, Y. Ziat, H. Belkhanchi, Z. Zarhri, Y. A. El Kadi, *Physica B: Condensed Matter* **2023**, *667*, 415216.
[32] J. W. Wafula, *Results Mater.* **2023**, *19*, 100413.
[33] S. A. Khandy, I. Islam, A. F. Wani, A. M. Ali, M. Sayed, M. Srinavasan, K. Kaur, *Physica B: Condensed Matter* **2024**, *677*, 415698.
[34] M. N. Rasul, T. Hu, M. Mehmood, F. Andleeb, M. S. Akbar, A. Manzoor, A. Hussain, *Mater. Sci. Semicond. Process.* **2024**, *172*, 108024.
[35] D. Bahara, S. Al-Qaisi, B. Akila, A. Dutta, T. Mundad, A. S. Alofi, Y. Bakkour, *Int. J. Quantum Chem.* **2024**, *124*, e27375.
[36] P. Blaha, K. Schwarz, P. Sorantin, S. Trickey, *Comput. Phys. Commun.* **1990**, *59*(2), 399–415, https://doi.org/ 10.1016/0010-4655(90) 90187–6.
[37] P. Hohenberg, W. Kohn, *Phys. Rev.* **1964**, *136*, B864.
[38] F. Belkharroubi, M. Ameri, D. Bensaid, M. Noureddine, I. Ameri, S. Mesbah, Y. Al-Douri, *J. Magn. Magn. Mater.* **2018**, *448*, 208–220.
[39] B. Nour-eddine, F. Belkharroubi, I. Ameri, L. Blaha, B. Abdelghani, D. Lamia, M. Bourdim, A. Tebboune, M. Belkaid, M. Ameri, *Mater. Today Commun.* **2022**, *33*, 104277.
[40] M. Ameri, F. Belkharroubi, I. Ameri, Y. Al-Douri, B. Bouhafs, F. Z. Boufadi, A. Touia, K. Boudia, F. Mired, *Mater. Sci. Semicond. Process.* **2014**, *26*, 205–217.
[41] S. Laroussi, F. Belkharroubi, I. Ameri, F. L. Blaha, A. Saim, A. Maizia, M. Ameri, Y. Al-Douri, *Emergent Mater.* **2022**, *5*(2), 537–551.
[42] F. Belkharroubi, F. Khelfaoui, K. Amara, N. Marbouh, M. Ameri, Y. Si Abderrahmane, *Physica B: Condensed Matter* **2019**, *557*, 56–62.
[43] B. Asma, F. Belkharroubi, A. Ibrahim, B. Lamia, A. Mohammed, W. Belkilali, Y. Al-Douri, *Emergent Mater.* **2021**, *4*(6), 1769–1783.
[44] F. Belkharroubi, M. Bourdim, A. Maizia, N. Belmiloud, F. Khelfaoui, Z. Smahi, K. Boudia, M. Benchehima, S. Azzi, M. Ameri, Y. Al-Douri, A. Abu-Odeh, *Philos. Mag.* **2023**, *103*(11), 1090–1114..
[45] M. K. Zoubir, F. Belkharroubi, K. Boudia, I. Ameri, L. F. Blaha, Y. Al-Douri, *Mater. Test.* **2021**, *63*(6), 537–542.
[46] Blaha, P. Schwarz, K. Madsen, G. K. H., Kvasnicka, D. and Luitz, J. (2001) WIEN2k: An Augmented Plane Wave plus Local Orbitals Program for Calculating Crystal Properties. Technische Universitat, Wien, Austria.
[47] J. P. Perdew, K. Burke, M. Ernzerhof, *Phys. Rev. Lett.* **1996**, *77*(18), 3865.
[48] M. Ayad, F. Belkharroubi, F. Z. Boufadi, M. Khorsi, M. Zoubir, M. Ameri, I. Ameri, Y. Al-Douri, K. Bidai, D. Bensaid, *Indian J. Phys.* **2020**, *94*, 767–777.
[49] A. Maizia, F. Belkharroubi, M. Bourdim, F. Khelfaoui, S. Azzi, K. Amara, *SPIN* **2020**, *10*, 2050026.
[50] U. Kreibig, *Z. Phys.* **1970**, *234*, 307–318.
[51] V. Lucarini, J. J. Saarinen, K. E. Peiponen, E. M. Vartiainen, *Kramers-Kronig relations in optical materials research*. Vol. 110. Springer Science & Business Media, **2005**.
[52] K. Lathrop, B. Carlson, *J. Comput. Phys.* **1966**, *1*(2), 173–197.
[53] H. J. Monkhorst, J. D. Pack, *Phys. Rev. B* **1976**, *13*(12), 5188.
[54] J. Kapil, P. Shukla, A. Pathak, *Eur. Phys. J. Plus* **2024**, *139*(5), 377.
[55] D.-E. Missoum, K. Bencherif, D. Bensaid, *Eur. Phys. J. B* **2023**, *96*(12), 160.
[56] F. D. Murnaghan, *Proc. Natl. Acad. Sci. USA* **1944**, *30*(9), 244–247.
[57] F. Sofrani, K. Boudia, F. Khelfaoui, M. Hamlat, A. Bouhemadou, A. Lorf, A. Hachilif, F. Belkharroubi, A. Slamani, *Indian J. Phys.* **2023**, *97*(13), 3875–3885.
[58] F. Benaddi, F. Belkharroubi, N. Ramdani, M. Ameri, S. Haouari, I. Ameri, L. Drice, S. azzi, Y. Al-Douri, *Emergent Mater.* **2021**, *4*(6), 1745–1760.
[59] M. J. Mehl, *Physical Review B: Condensed Matter* **1993**, *47*, 2493–2500.
[60] D. C. Wallace, H. Callen, *Am. J. Phys.* **1972**, *40*(11), 1718–1719.
[61] M. Born, K. Huang, *Dynamical theory of crystal lattices*. Oxford university press, **1996**.
[62] E. Schreiber et al., *Elastic constants and their measurement*, McGraw-Hill, New York **1975**, 747–748.
[63] M. Born, K. Huang, *Dynamical Theory of Crystal Lattice*, Oxford University Press, Oxford **1954**.
[64] a) D. G. Pettifor, *Mater. Sci. Technol.* **1992**, *18*, 345–349; b) Y. Pan, S. L. Wang, C. M. Zhang, *Vacuum.* **2018**, *151*, 205–208; c) L. Hao, R. Khenata, X. Wang, T. Yang, *J. Electron. Mater.* **2019**, *48*, 6222–6230.
[65] R. Hill, *Proc. Phys. Soc. A.* **1952**, *65*, 349.
[66] S. M. Laoufi, A. Touia, M. Ameri, I. Ameri, F. Boufadi, K. Boudia, A. Slamani, F. Belkharroubi, Y Al-Douri, *Optik* **2016**, *127*(18), 7382–7393.
[67] D. H. Chung, W. R. Buessem, *J. Appl. Phys.* **1967**, *38*(5), 2010–2012.
[68] S. Shrikanth, R. Prasad, S. Neelakantan, *J. Appl. Phys.* **2021**, *129*(21), 215101.
[69] S. Sing, R. Kumar, *J. Alloys Compd.* **2017**, *722*, 544–548.
[70] A. Benamer, Y. Medkour, S. Sâad Essaoud, S. Chaddadi, A. Roumili, *Solid State Commun.* **2021**, *331*, 114305.
[71] M. K. Butt, M. Yaseen, I. A. Bhatti, J. Iqbal, Misbah, A. Murtaza, M. M. Anazy, M. H. Alhossainy, A. Laref, *J. Mater. Res. Technol.* **2020**, *9*, 16488–16496.
[72] M. W. Qureshi, X. Ma, G. Tang, R. Paudel, *Materials* **2020**, *13*(22), 5148.
[73] S. F. Pugh, *London, Edinb. Dublin Philos. Mag. J. Sci.* **1954**, *45*(367), 823–843.
[74] N. Mehmood, R. Ahmad, G. Murtaza, *J. Supercond. Nov. Magn.* **2017**, *30*, 2481–2488.
[75] S. U. Zaman, N. Rahman, M. Arif, M. Saqib, M. Husain, E. Bonyah, Z. Shah, S. Zulfiqar, A. Khan, *AIP Adv.* **2021**, *11*(1), 015204.
[76] D. Behera, S. Al-Qaisil, M. Manzour, Mumtaz, et al., *Mater. Sci. Eng. B* **2023**, *297*, 116765.
[77] H. Arquam, A. Srivastava, K. Meena, L. Kunjee, et al., *Physica Status Solidi B* **2024**, *261*, 2300571.
[78] M. Khan, A. Kashyap, A. Solanki, T. Nautiyal, S. Auluck, *Phys. Rev. B* **1993**, *48*(23), 16974.
[79] Y. Ammari, E. K. Hlil, *Chem. Pap.* **2021**, *75*(7), 3197–3205.
[80] M. Ullah, S. Khan, A. Laref, G. Murtaza, *Philos. Mag.* **2020**, *100*(6), 768–781.
[81] M. Irfan, M. A. Kamran, S. Azam, M. WaqasIqbal, T. Alharbi, A. Majid, S. BinOmran, *J. Mol. Graphics Modell.* **2019**, *92*, 296–302.
[82] P. E. Blöchl, O. Jepsen, O. K. Andersen, *Phys. Rev. B* **1994**, *49*(23), 16223.
[83] T. Geleta, A. Tesfaye, D. Behera, R. Sharma, et al., *RSC Adv.* **2024**, *14*, 4165–4178.
[84] P. Ravindran, A. Delin, B. Johansson, O. Eriksson, J. Wills, *Phys. Rev. B* **1999**, *59*(3), 1776.
[85] H. R. Philipp, H. Ehrenreich, *Phys. Rev.* **1963**, *129*(4), 1550.
[86] D. J. Singh, L. Nordstrom, *Planewaves, Pseudopotentials, and the LAPW method*, Springer Science & Business Media, **2006**.
[87] A. Özmen, Y. Yakar, B. Çakır, Ü. Atav, *Opt. Commun.* **2009**, *282*(19), 3999–4004.
[88] K. F. Mak, M. Y. Sfeir, Y. Wu, C. H. Lui, J. A. Misewich, T. F. Heinz, *Phys. Rev. Lett.* **2008**, *101*(19), 196405.

[89] T. Stauber, N. Peres, A. Geim, *Phys. Rev. B* **2008**, *78*(8), 085432.
[90] A. Reshak, *RSC Adv.* **2016**, *6*(100), 98197–98207.
[91] O. Sadouki, F. Khelfaoui, F. Fontaine-Vive, K. Boudia, H. Hocine, E. Sert, A. R. Benrekia, M. Hamlat, A. Slamani, F. Belkharroubi, K. Amara, *J. Electron. Mater.* **2023**, *52*(10), 6778–6790.
[92] K. F. Brennan, *The physics of semiconductors: with applications to optoelectronic devices*, Cambridge university press, **1999**.
[93] A. Slamani, F. Khelfaoui, O. Sadouki, A. Bentayeb, K. Boudia, F. Belkharroubi, Slamani, *Emergent Mater.* **2023**, *6*(2), 681–690.
[94] Y. Benazouzi, H. Rozale, M. B. Hacene, M. Khethir, A. Chahed, D. Lucache, *Annals of West University of Timisoara-Physics Ann. West Univ. Timisoara-Phys.* **2019**, *61*(1), 44–55.
[95] D. Shrivastava, S. P. Sanyal, *J. Alloys Compd.* **2019**, *784*, 319–329.

Manuscript received: September 23, 2024
Revised manuscript received: December 12, 2024
Accepted manuscript online: February 3, 2025
Version of record online: ■■, ■■

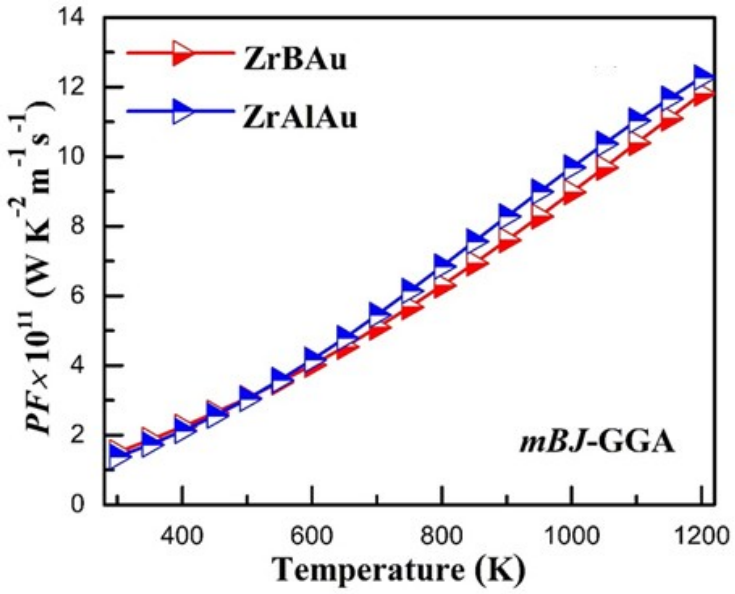

R. N. El Imene Bennoui, W. Adli, Y. Al-Douri, F. Belkharroubi, F. Sidjilani, A. Bentayeb, F. Khelfaoui, N. Belmiloud, S. A. Bendella, L. Alagui, A. S. A. Dib, M. N. Belkaid*

1 – 24

Valence Electron Count-Based Density Functional Theory to Investigate Structural Stability, Optoelectronic and Thermoelectric Properties of New p-Type Half-Heusler ZrYAu (Y = B, Al) Alloys

Full-potential linearized augmented plane wave is employed to investigate structural, mechanical, optoelectronic and thermoelectric properties of novel half-Heusler ZrYAu alloys (where Y = B or Al) with valence electron count (VEC) of 8. Both are mechanically stable, display semiconducting behavior and exhibit high optical conductivity. However, both are effective absorbers of UV light and demonstrate significant p-type thermoelectric power.